CHEMISTRY
A EUROPEAN JOURNAL

FULL PAPER

DOI: 10.1002/chem.201201772

Iridium-Catalyzed Allylic Substitutions with Cyclometalated Phosphoramidite Complexes Bearing a Dibenzocyclooctatetraene Ligand: Preparation of (π-Allyl)Ir Complexes and Computational and NMR Spectroscopic Studies

Jevgenij A. Raskatov, Mascha Jäkel, Bernd F. Straub, Frank Rominger, and Günter Helmchen*[a]

Abstract: (π-Allyl)Ir complexes derived from dibenzocyclooctatetraene and phosphoramidites by cyclometalation are effective catalysts for allylic substitution reactions of linear monosubstituted allylic carbonates. These catalysts provide exceptionally high degrees of regioselectivity and allow the reactions to be run under aerobic conditions. A series of (π-allyl)Ir complexes were prepared and characterized by X-ray crystal structure analyses. An allylic amination with aniline displayed different resting states depending on the presence of a strong base. DFT calculations were carried out on the mechanistic aspects of these reactions. The results suggest that for the (π-allyl)Ir complexes, the formation and reactions with nucleophiles proceed with comparable rates.

Keywords: allylic substitution · asymmetric catalysis · iridium · phosphoramidites · reaction mechanisms

Introduction

From 1997[1] onwards, the Ir-catalyzed allylic substitution reaction has been developed into a useful tool for organic synthesis. The reaction allows branched allylic derivatives **2** to be prepared from readily available linear allylic derivatives, most often allylic carbonates **1** (Scheme 1).[2] Catalysts for this reaction are usually prepared by base-induced C–H activation from $[\{Ir(cod)Cl\}_2]$ (cod = cycloocta-1,5-diene).[3,4] The scope of the reaction with respect to the nucleophile is very broad; C-, N-, O-, and S-nucleophiles having been used successfully, and enantioselectivities are usually high.[5] Intramolecular reactions are facile and can be carried out at concentrations of 1 M and higher without noticeable competing polymerization.[3,6]

Regioselectivities **2**:**3** are high with sp^2 substituents R, but can be as low as about 70:30 with aliphatic substituents R. We have introduced catalysts derived from $[\{Ir(dbcot)Cl\}_2]$ (dbcot = dibenzocyclooctatetraene),[7] which generally induce superior regioselectivity and, in addition, allow the substitution reactions to be run under aerobic conditions. Dbcot can be conveniently prepared on a multigram scale.[8] Several successful applications of these catalysts have been reported.[9] The unusual properties of these new catalysts have induced us to study the mechanistic aspects of their reactions. Herein, we report these results, including DFT calculations and catalyst optimization studies.

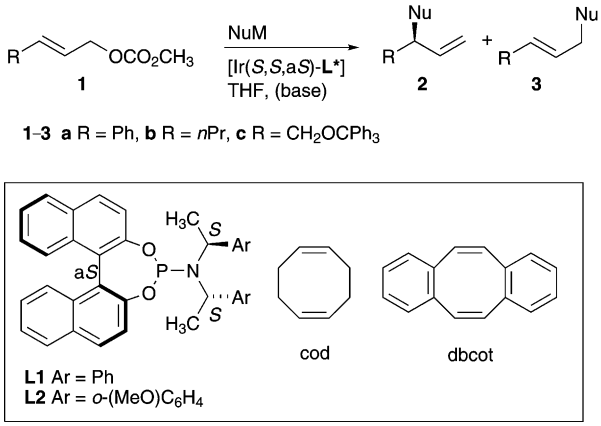

Scheme 1. Ir-catalyzed allylic substitution reactions and the most commonly used ligands.

Current views on catalyst activation and the catalytic cycle of the reaction are shown in Scheme 2.[4,10,11] In the first step, mixing $[\{Ir(diene)Cl\}_2]$ with a phosphoramidite (**L**) yields complexes of the well-known type **C1**. Treatment of **C1** with base effects C–H activation to give iridacycles of type **C2**, which have been characterized previously.[4] Entry into the catalytic cycle likely proceeds via a 16 valence electron (VE) complex of type **C3**, which has so far not been isolated. Next, coordination of the substrate to form **C4** and oxidative addition to give the crucial π-allyl complexes **C5**

[a] Dr. J. A. Raskatov, M. Jäkel, Prof. Dr. B. F. Straub, Dr. F. Rominger, Prof. Dr. G. Helmchen
Organisch-Chemisches Institut
Ruprecht-Karls-Universität Heidelberg
Im Neuenheimer Feld 270, 69120 Heidelberg (Germany)
Fax: (+49) 6221-544205
E-mail: g.helmchen@oci.uni-heidelberg.de

Supporting information for this article is available on the WWW under http://dx.doi.org/10.1002/chem.201201772.

© 2012 Wiley-VCH Verlag GmbH & Co. KGaA, Weinheim
WILEY ONLINE LIBRARY
These are not the final page numbers!

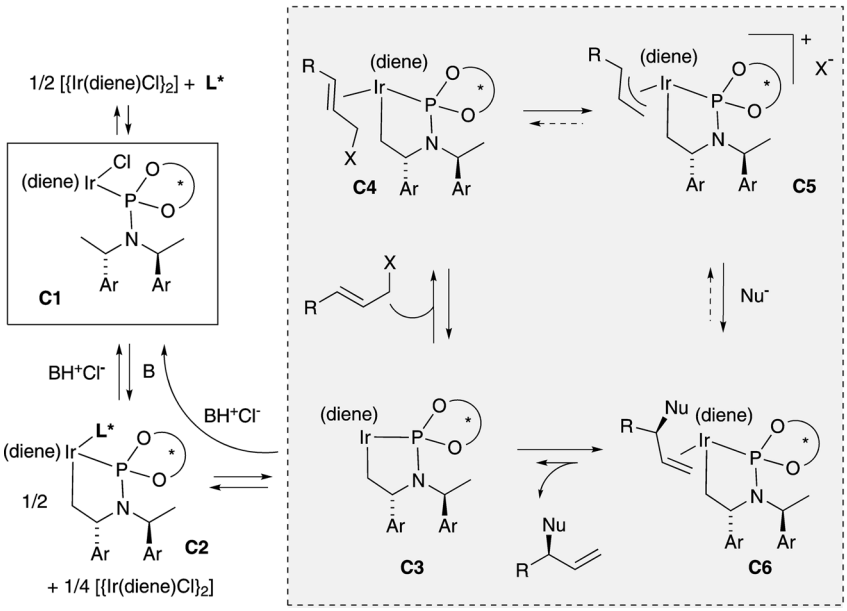

Scheme 2. Catalytic cycle of an allylic substitution reaction using a catalyst prepared in situ from compound **C1** by treatment with an amine base (B).

occurs. A wide variety of complexes **C5** with cod as diene ligand have been prepared (see below) and are active catalysts. Based on investigation of the reaction kinetics of allylic amination reactions, Hartwig and co-workers have postulated that the formation of the π-allyl complexes **C5**, in which the diene = cod, is reversible and endergonic,[10] while we have identified a π-complex as the resting state of an allylic alkylation reaction.[11] The reaction of **C5** with a nucleophile produces the olefin complexes **C6**. Such complexes have been observed by NMR spectroscopy. Depending mainly on the nucleophile, the π-allyl complex **C5** or the product complex **C6** have been observed as resting states of the reaction.

The steric course of the reaction, that is, the relationship between the configuration of the product and that of the catalyst, has previously been assessed for the step **C5**→**C6**, that is, the addition of the nucleophile at the π-allyl complex,[10,11] by DFT calculations. The correct configuration of the product was derived by using the simple argument that the nucleophile would preferentially add at the terminal carbon atom of the observed π-allyl complex, which was also found in the DFT calculations to be the most stable[11] and displayed the longer bond with Ir.

This argument is a problematic one in the case of Ir catalysis, because Ir^{III} complexes are kinetically inert and, thus, the fast equilibration of π-allyl complexes, which is typical for Pd^{II} complexes, is usually not valid for Ir complexes. It is necessary, therefore, to also investigate the formation of π-(allyl)Ir complexes, that is, the steps **C3**→**C4**→**C5**. This has now been carried out for a dbcot complex with the help of DFT calculations. The necessity to investigate the full set of steps is underlined by a very recent report by Madrahimov and Hartwig on the corresponding reactions with cod complexes.[10] Their complete determination of the kinetic data shows that the formation of the π-allyl intermediate determines the steric course of the substitution reaction. Recently, DFT calculations on the cyclometalation step of cod complexes have been published by You and coworkers.[5]

Results and Discussion

Preparation of (π-allyl)-(dbcot)Ir complexes

The (π-allyl)Ir complexes were prepared according to a method developed recently by us for complexes **C5** with cod as diene ligand.[11] This very convenient method also allowed a variety of dbcot complexes to be prepared in excellent yields of 84–98% [Eq. (1)]. The method involves the simple treatment of a solution of [{Ir(dbcot)Cl}$_2$], **L**, and allylic carbonate **1** in THF with a soluble silver salt, usually AgOTf, followed by the removal of AgCl by filtration:

$$[\{Ir(dbcot)Cl\}_2]+\mathbf{L}+\mathbf{1}+AgOTf \rightarrow \mathbf{C5}+AgCl+CO_2+CH_3OH \quad (1)$$

These complexes (Figure 1) are stable against water and air, can be purified by column chromatography on silica gel, and can be stored for extended periods of time. Several complexes were characterized by X-ray crystal-structure analysis (see below).

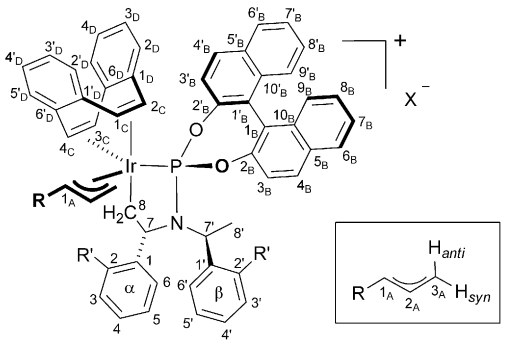

Figure 1. Atom numbering in complexes **C5**.

The dbcot complexes prepared in the course of our investigation, as well as the previously elucidated mechanism for

 © 2012 Wiley-VCH Verlag GmbH & Co. KGaA, Weinheim

These are not the final page numbers!

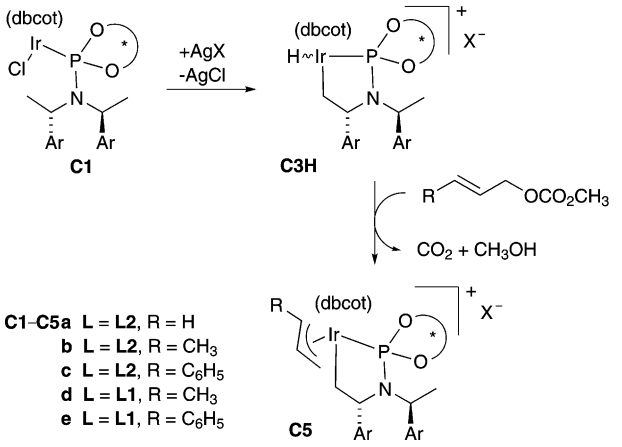

Scheme 3. Synthesis of (π-allyl)Ir complexes **C5a**–**C5e** (X = OTf) from simple components.

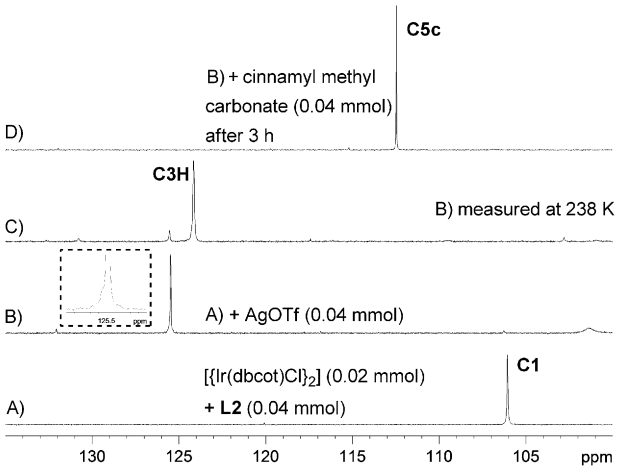

Figure 2. Preparation of compound **C5c**. $^{31}P\{^1H\}$ NMR spectra: A) [{Ir(dbcot)Cl}$_2$] (0.02 mmol)+(*R*,*R*,a*R*)-**L2** (0.04 mmol) in [D$_8$]THF (0.5 mL) after 30 min at RT; B) addition of AgOTf (0.04 mmol) to solution (A) at RT; C) mixture (B) measured at 238 K; D) addition of cinnamyl methyl carbonate (0.04 mmol) to solution (B), recorded after 3 h at RT.

the formation of the corresponding cod complexes,[11] are shown in Scheme 3. The formation of complex **C5c** was monitored by ^{31}P NMR spectroscopy (Figure 2). Initially, complex **C1** (Ar = *o*-(MeO)C$_6$H$_4$) was prepared by mixing [{Ir(dbcot)Cl}$_2$] and ligand **L2** in THF (Figure 2A).[7] Then, AgOTf was added, which caused a precipitation of AgCl. The resultant solution displayed an asymmetric signal at $\delta_{31P} = 125$ ppm at room temperature (Figure 2B). Upon cooling, this signal split into two peaks with an intensity ratio of 9:1 (Figure 2C). The corresponding ^1H NMR spectrum (not shown) displayed Ir–H resonances at $\delta = -21.1$ ppm and $\delta = -18.5$ ppm with an intensity ratio of 10:1. Accordingly, lines in Figure 2B and 2C were assigned to the diastereomers of the complex **C3H** (Ar = *o*-(MeO)C$_6$H$_4$). Solution B (Figure 2), which contained [{Ir(dbcot)Cl}$_2$], ligand **L2**, and AgOTf in THF, was treated with cinnamyl methyl carbonate (**1a**). Within 3 h, the ^{31}P NMR resonances of the hydrides vanished and a singlet that corresponded to complex **C5c** remained (Figure 2D).

Allylic substitution reactions with complexes C5 as catalysts

These new allyl complexes were probed as catalysts under salt-free conditions[12] with a set of representative substrates, and the results were compared with those achieved with catalysts formed in situ (Table 1). The configurational relationships given in Scheme 1 were found to be valid for all of the reactions. As a rule, isolated complexes **C5** induced slightly

Table 1. Allylic substitution reactions (according to Scheme 1) with isolated or in-situ-generated complexes **C5** as catalysts (solvent: THF, base: TBD = 1,5,7-triazabicyclo[4.4.0]dec-5-ene).[a]

Entry	R	Pronucleophile/nucleophile	Catalyst	*t* [h]	Yield **2**+**3** [%][b]	**2**/**3**[c]	*ee* [%][d]
1	Ph	$CH_2(CO_2CH_3)_2$	in situ[e]	2	96	99:1	99
2	Ph	$CH_2(CO_2CH_3)_2$	**C5c**[e]	1	91	99:1	99
3[g]	Ph	$CH_2(CO_2CH_3)_2$	**C5c**	4	91	98:2	96
4	Ph	$HN(Boc)_2$	in situ[e]	18	63	95:5	99
5	Ph	$HN(Boc)_2$	**C5b**[e]	2	70	93:7	98
6[g]	Ph	$HN(Boc)_2$	**C5b**	3	93	94:6	98
7	Ph	$PhNH_2$	in situ[e]	18	88	92:8	98
8	Ph	$PhNH_2$	**C5b**[e]	3.5	73	92:8	95
9	Ph	$PhNH_2$	**C5b**[f]	1	79[f]	0:100	–
10[h]	*n*Pr	$CH_2(CO_2CH_3)_2$	in situ	3.5	90	97:3	94
11[h]	*n*Pr	$CH_2(CO_2CH_3)_2$	**C5b**[e]	3.5	91	97:3	94
12[g]	*n*Pr	$CH_2(CO_2CH_3)_2$	**C5b**	19	64	97:3	93
13[h]	CH_2OCPh_3	$CH_2(CO_2CH_3)_2$	in situ[e]	1	80	92:8	93
14[h]	CH_2OCPh_3	$CH_2(CO_2CH_3)_2$	**C5c**[e]	1	83	93:7	93
15[g,h]	CH_2OCPh_3	$CH_2(CO_2CH_3)_2$	**C5b**	3	73	96:4	93

[a] Reactions were carried out under "salt-free conditions" (see ref. [12]). Catalyst in situ: a solution of [{Ir(dbcot)Cl}$_2$] (2 mol%), ligand **L2** (4 mol%), and dry TBD (8 mol%) was stirred in dry THF (0.5 mL) at RT for 10 min. Isolated complex as the catalyst: compound **C5** (4 mol%) was dissolved in dry THF (0.5 mL). Allylic substitution reaction: a solution of the catalyst was treated with carbonate **1** (0.5 mmol), the nucleophile or pronucleophile (0.6 mmol), and, when compound **C5** was used as the catalyst, TBD (8 mol%). [b] Yield of isolated product. [c] Determined by ^1H NMR spectroscopy of the crude products. [d] Determined by chiral HPLC (see the Experimental Section). [e] The reaction was carried out with a catalyst that was derived from *ent*-**L2**. [f] The reaction was carried out without additional base. Besides compound **3a**, 13% of linear *N*,*N*-dicinnamylaniline was isolated. [g] The reaction was carried out under aerobic conditions. [h] The reaction was carried out at 50 °C. Boc = *tert*-butoxycarbonyl.

© 2012 Wiley-VCH Verlag GmbH & Co. KGaA, Weinheim

faster reactions than the in-situ-generated catalysts, and the regioselectivities (^{1}H NMR spectroscopy) and enantioselectivities (HPLC) were the same within the range of precision of the measurements. We had earlier noted that reactions that were catalyzed by dbcot complexes could be run under aerobic conditions (Table 1, entries 3, 6, 12, and 15), which is not possible with the corresponding cod complexes.

Allylic substitution reactions catalyzed by cod complexes are usually run in THF as solvent, because more polar solvents are detrimental with respect to enantioselectivity.[13] The generally enhanced robustness of the dbcot complexes allows the reactions to be run in a very broad range of solvents, as is apparent from the results for an alkylation reaction (Table 2). Regioselectivity is practically independent of the solvent, whereas enantioselectivity is eroded in DMF and, notably, in DMSO, but not in MeCN. Low selectivity with DMSO was also observed by us for a hydroxylation reaction,[9c] whereas a beneficial effect of this solvent has been reported for allylic amination reactions run under aerobic conditions.[9b]

Table 2. Influence of the solvent on the alkylation reaction (according to Scheme 1, carbonate **1c**, dimethyl malonate as the pronucleophile) by using complexes **C5b** and **C5d** as the catalyst.[a]

Entry	Solvent	Catalyst	t [h]	Yield **2**+**3** [%][b]	**2**/**3**[c]	*ee* [%][d]
1	CH_3CN	**C5b**	1	86	94:6	96
2	CH_3CN	**C5d**	1.5	74	94:6	95
3	DMF	**C5b**	1	88	92:8	94
4	DMF	**C5d**	1.5	74	n.d.	90
5	DMSO	**C5b**[e]	3	77	92:8	92
6	DMSO	**C5d**	5	78	92:8	88
7	*i*PrOH	**C5b**	1.5	74	93:7	90
8	*i*PrOH	**C5d**	2	80	94:6	93
9	1,2-dichloroethane	**C5b**	1.5	74	95:5	95
10	1,2-dichloroethane	**C5d**	2	82	96:4	95
11	toluene	**C5b**[e]	1.5	75	94:6	96
12	toluene	**C5d**	7	85	94:6	96
13	1,4-dioxane	**C5b**	1.5	73	94:6	94

[a] Reactions were carried out at 50 °C: Complex **C5** (4 mol %) was dissolved in absolute solvent (0.5 mL) and carbonate **1c** (0.25 mmol), $CH_2(CO_2CH_3)_2$ (0.3 mmol), and dry TBD (8 mol %) were added. [b] Yield of isolated product. [c] Determined by ^{1}H NMR spectroscopy of the crude products. [d] Determined by chiral HPLC (see the Experimental Section). [e] The reaction was carried out with *ent*-**C5b**.

As described below, DFT calculations were carried out on the course of the allylic substitution reaction with allylic trimethylammonium ions as reaction partners. Metal-catalyzed allylic substitution reactions with allylic ammonium salts have been reported with Pd but not with Ir catalysts;[14] therefore, we have investigated the allylic amination of the ammonium salt **4**, as an example (Table 3), to assess whether the results are similar to those achieved with the typically used allylic carbonates. Catalysts containing a cod or dbcot ancillary ligand were probed. Under kinetically controlled conditions and short reaction times (6 h), the regio- and enantioselectivities, as well as the steric course of the reactions, were similar to those obtained with carbonates. However, the reversibility of the reaction was apparent by the formation of linear product **3** upon extending the reaction time to 24 h. From a practical point of view, ammonium salts are clearly inferior to carbonates as substrates.

Table 3. Allylic amination reactions with an allylic trimethylammonium salt as the substrate.[a]

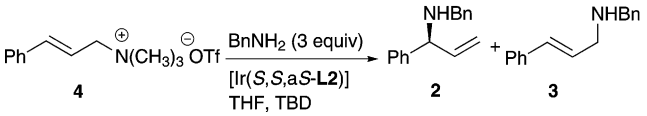

4 **2** **3**

Entry	Catalyst	Diene	t [h]	Yield **2**+**3** [%][b]	**2**/**3**[c]	*ee* [%][d]
1	in situ	cod	6	43	93:7	94
2	in situ[e]	cod	24	69	80:20	94
3	**C5f**[f]	cod	6	57	95:5	94
4	in situ	dbcot	6	37	70:30	89
5	in situ	dbcot	24	52	30:70	80
6	**C5b**	dbcot	6	58	91:9	92
7	**C5b**	dbcot	24	62	82:18	85

[a] Reaction conditions: At RT, either a solution of [{Ir(diene)Cl}$_2$] (2 mol %), ligand **L2** (4 mol %), and dry TBD (8 mol %) in dry THF (1.25 mL) (in situ procedure) or a solution of compound **C5** (4 mol %) and dry TBD (8 mol %) was prepared in dry THF (1.25 mL); then, ammonium salt **4** (0.25 mmol) and $BnNH_2$ (0.75 mmol) were added. [b] Yield of isolated product. [c] Determined by ^{1}H NMR spectroscopy of the crude products. [d] Determined by chiral HPLC (see the Experimental Section). [e] The reaction was carried out with *ent*-**L2**. [f] **C5f** = [Ir(cod)(*C*,*P*-**L2**)(crotyl)]OTf; for its preparation, see ref. [11].

Resting state of an allylic amination reaction upon the use of a (π-allyl)(dbcot)Ir complex as a catalyst

The resting state of allylic substitution reactions catalyzed by cod complexes has been investigated by the Hartwig group[10] and by our group.[11] For the allylic amination reaction with aniline, complex **C6** (diene = cod) was observed as the resting state, which led Hartwig and co-workers to conclude that the formation of the (π-allyl)Ir complexes is endergonic and reversible. For that work, in situ catalysts were used. However, for an alkylation reaction with dimethyl malonate that was catalyzed with an isolated allyl complex (**C5**, diene = cod), we observed the allyl complex to be the resting state. Herein, we have investigated the reaction of aniline with cinnamyl methyl carbonate (**1a**) using the dbcot complex **C5b** as the catalyst; we found that both scenarios were observable for a given set of substrates, depending on the presence/absence of a strong base.[15]

Thus, when the reaction was run with catalyst **C5b** without an additional base, the linear product **3a** was formed. Initially, up to 10 % of branched product **2a** was observed (by ^{1}H NMR spectroscopy), which vanished during the course of the reaction, that is, compound **3a** is the product under thermodynamic control. Clearly, the intermediary branched ammonium salt and/or the corresponding Ir complex undergoes a further amination reaction (Scheme 4). ^{31}P NMR (Figure 3), as well as ^{1}H NMR spectra were measured during the reaction and after the amination step had been completed. Addition of carbonate **1a** and aniline to the sol-

© 2012 Wiley-VCH Verlag GmbH & Co. KGaA, Weinheim

These are not the final page numbers!

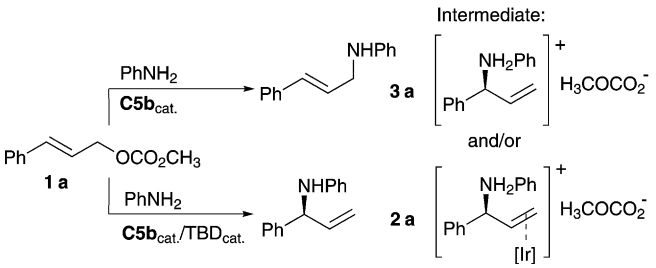

Scheme 4. Influence of base on the reaction of aniline with carbonate **1a**.

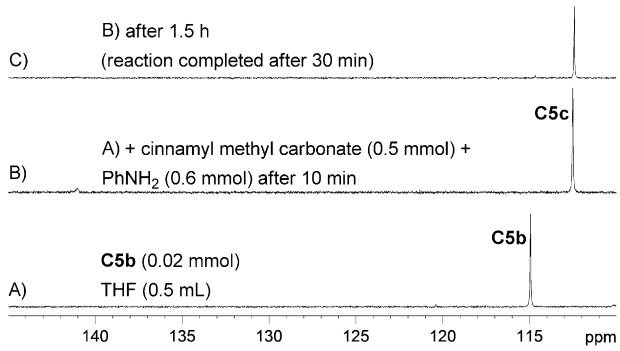

Figure 3. Allylic amination without additional base, according to Scheme 4; $^{31}P\{^1H\}$ NMR spectra: A) compound **C5b** (0.02 mmol) in $[D_8]$THF (0.5 mL); B) addition of carbonate **1a** (0.5 mmol) and $PhNH_2$ (0.6 mmol) to solution (A), recorded after 10 min at RT; C) recorded after 1.5 h at RT, the reaction was complete (by ^1H NMR spectroscopy) after 30 min.

ution of the crotyl complex **C5b** (Figure 3 A) caused the formation of cinnamyl complex **C5c** ($\delta_{31P}=112.4$ ppm, Figure 3 B). This intermediate persisted throughout the amination reaction. A small signal at $\delta_{31P}=141.0$ ppm likely belongs to the Ir complex **C6** of the branched product (see below). A signal corresponding to the olefin complex of the linear product was not observed.

Next, the course of the reaction was investigated with the addition of a catalytic amount of base. Weak bases, such as triethylamine, had no significant effect; however, strong bases TBD (1,5,7-triazabicyclo[4.4.0]dec-5-ene) and DBU (1,8-diazabicyclo[5.4.0]undec-7-ene) completely changed the course of the reaction in that the branched product **2a** was predominantly formed (Table 1). A representative set of ^{31}P NMR spectra is shown in Figure 4. Addition of aniline to a mixture of complex **C5b**, cinnamyl methyl carbonate, and

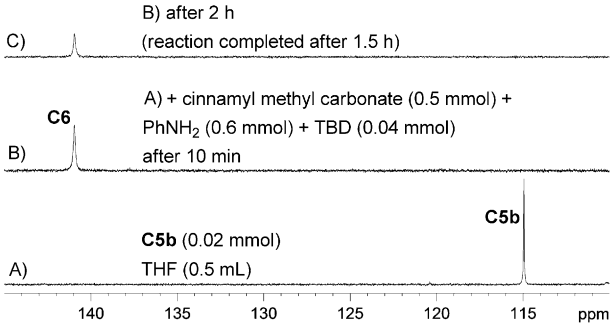

Figure 4. Allylic amination according to Scheme 4 with an additional catalytic amount of TBD; $^{31}P\{^1H\}$ NMR spectra: A) compound **C5b** (0.02 mmol) in $[D_8]$THF (0.5 mL); B) addition of carbonate **1a** (0.5 mmol), $PhNH_2$ (0.6 mmol), and TBD (0.04 mmol) to solution (A), recorded after 10 min at RT; C) recorded after 2 h at RT, the reaction was complete (by ^1H NMR spectroscopy) after 1.5 h.

a catalytic amount of TBD led to the formation of a species displaying a signal at $\delta_{31P}=141.0$ ppm, which persisted throughout the reaction. In analogy to the corresponding reaction of the cod complexes, this new species is presumably olefin complex **C6** (diene = dbcot, R = Ph; Scheme 2). Quite clearly, fast deprotonation of the intermediary branched ammonium salt leads to a stable olefin complex (**C6**) under kinetic control.

X-ray crystal structures of the (π-allyl)Ir complexes

High-resolution crystal structures were obtained for complexes [Ir(dbcot)(*C*,*P*-**L2**)(allyl)]$^+$ (**C5a**), [Ir(dbcot)(*C*,*P*-**L2**)(crotyl)]$^+$ (**C5b**), [Ir(dbcot)(*C*,*P*-**L2**)(cinnamyl)]$^+$ (**C5c**), [Ir(dbcot)(*C*,*P*-**L1**)(crotyl)]$^+$ (**C5d**), and [Ir(dbcot)(*C*,*P*-**L1**)(cinnamyl)]$^+$ (**C5e**); the counterion was triflate in all cases (Scheme 3). Selected geometric parameters are listed in Table 4.

The five-membered iridacycle adopts envelope conformation A (Figure 5) in all of the crystal structures (Figure 6). This parallels well with the previous results obtained for a broad range of cod analogues.[10,11] For complexes **C5a** and **C5b**, a second rotamer (A′) was observed, in which the aryl ring α was flipped (Figure 5, conformer A′). DFT calculations for complex **C5a** suggest that the conformer A′ is disfavored by 2.1 kcal mol^{-1} with respect to conformer A (see the Supporting Information). Therefore, the subsequent discussion of crystallographic parameters and the Computational

Table 4. Selected bond lengths [Å] and bond angles [°] in (π-allyl)Ir complexes **C5a**–**C5e**.

Complex[a]	Ir–$C1_A$	Ir–$C2_A$	Ir–$C3_A$	$C1_A$–$C2_A$	$C2_A$–$C3_A$	$C1_A$-$C2_A$-$C3_A$	P-Ir-CH_2	Sum of bond angles at N	τ(C8′-C7′-N-C7)	τ(Ir-C8-C7-C1)
C5a	2.245(6)	2.190(5)	2.221(6)	1.420(10)	1.399(10)	120.6(6)	76.6(2)	359.8	115.9	−149.0
C5b	2.346(4)	2.211(3)	2.190(3)	1.397(6)	1.417(6)	120.9(3)	76.1(1)	359.7	115.6	−152.2
C5c	2.397(4)	2.233(4)	2.204(4)	1.409(6)	1.424(6)	122.4(4)	74.3(1)	356.1	150.8	−167.2
C5d	2.359(3)	2.230(3)	2.204(4)	1.393(5)	1.434(5)	122.2(3)	76.9(1)	357.5	153.2	−164.4
C5e/1[a]	2.394(8)	2.223(7)	2.174(8)	1.385(11)	1.408(11)	121.4(8)	75.6(2)	357.2	139.9	−167.0
C5e/2[a]	2.408(7)	2.211(7)	2.174(8)	1.386(12)	1.415(11)	122.2(8)	76.0(2)	356.1	141.8	−169.5

[a] The designations "/1" and "/2" refer to independent molecules within the unit cell.

© 2012 Wiley-VCH Verlag GmbH & Co. KGaA, Weinheim

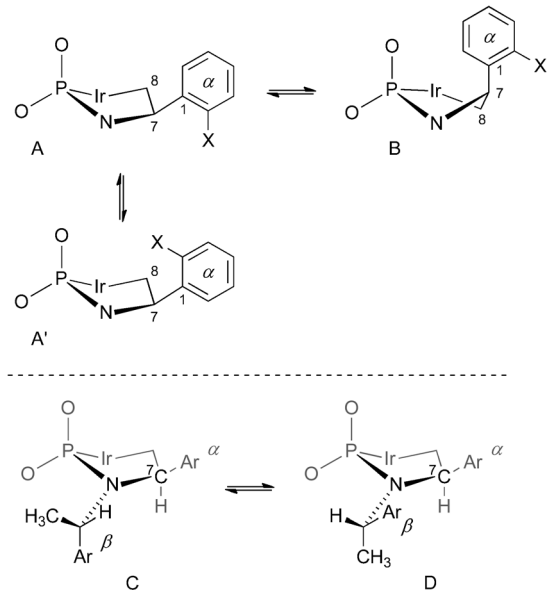

Figure 5. Conformations of the *C*,*P*-chelate ligand in complexes **C5** (Ar = *o*-(MeO)C_6H_4 or Ph).

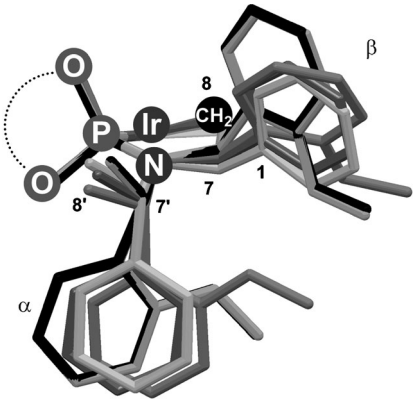

Figure 6. Superposition of segments of the crystal structures of (π-allyl)Ir complexes **C5**; the allylic fragment, dbcot, and BINOL are omitted for clarity. For a color Figure, see the Supporting Information.

Section are based exclusively on conformer A. The (β)arylethyl group was found in the conformation D (Figure 5) for all structures (Figure 6), again paralleling nicely the observations made for the cod complexes.

Concerning the allylic moiety, the crystal structure of cinnamyl complex **C5c** is discussed as an example (Figure 7) and subsequently compared with its analogues. The bonding of the cinnamyl moiety to iridium in complex **C5c** is distorted in that the Ir–$C1_A$ distance is substantially longer than the Ir–$C3_A$ distance (2.397 vs. 2.204 Å). The Ir–$C2_A$ distance (2.233 Å) is very similar to that of Ir–$C3_A$. The allylic bonds $C1_A$–$C2_A$ and $C2_A$–$C3_A$ are not significantly different from each other. The structure possesses strong resemblance to the analogue **C5e** derived from ligand **L1**. A substantial difference between complexes **C5c** and **C5e** was only found with the 1-phenylethyl substituent, for which the torsional angles were 150.8° (**C5c**), 139.9° (**C5e**/**1**), and 141.8° (**C5e**/**2**).

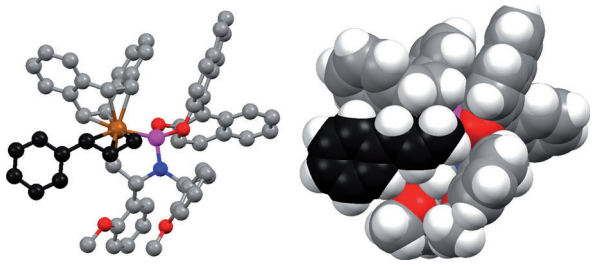

Figure 7. Crystal structure of complex **C5c** represented as ball-and-stick (left) and CPK models (right).

Given that this is a rotation about a single bond (Figure 5, conformers C and D), this variation is not likely to be associated with significant energetic differences and is possibly rooted in different crystal packing forces between the crystals.

The crotyl complexes **C5b** (**L2**) and **C5d** (**L1**) display a slightly less pronounced (but still significant) distortion; again, Ir–$C1_A$ is longer than Ir–$C3_A$. On the other hand, the unsubstituted allyl moiety in complex **C5a** was essentially symmetric with respect to its bonding to iridium (Ir–$C1_A$ = 2.245, Ir–$C3_A$ = 2.221 Å). The torsional angle C8′-C7′-N-C7 spans a rather broad range between 115.6° (**C5b**) and 153.2° (**C5d**; Figure 6).

The distances between the iridium atom and the allyl moiety in complexes **C5b** and **C5c** were compared with those of their cod analogues (Figure 8). For both complexes **C5b** and **C5c**, the bond lengths in the dbcot structures and their corresponding cod structures are similar (Table 5). Some variation in the orientation of the free α- and β-aryl rings is again apparent.

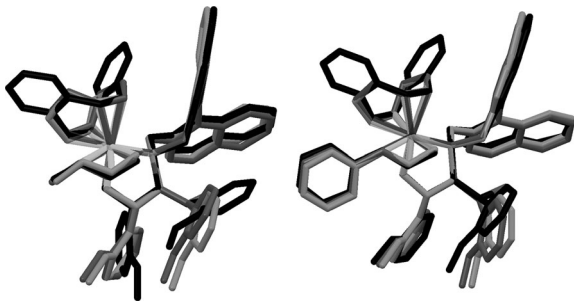

Figure 8. Comparison of the structures of analogous cod and dbcot complexes. Left: superposition of the structures of crotyl complex **C5b** with its cod analogue (two crystallographically independent structures);[11b] right: an analogous superposition of complex **C5c** and its cod analogue (two crystallographically independent structures).[11b] For a color Figure, see the Supporting Information.

DFT calculations

Computations were carried out on various structures with reference to the catalytic cycle shown in Scheme 2 (R = CH_3, diene = dbcot, and Ar = *o*-(MeO)C_6H_4).

© 2012 Wiley-VCH Verlag GmbH & Co. KGaA, Weinheim

These are not the final page numbers!

Table 5. Comparison of the iridium–allyl distances [Å] for complexes **C5b** and **C5c** with their cod analogues (**C5f** and **C5g**, respectively).

Complex[a]	Ir–C1$_A$	Ir–C2$_A$	Ir–C3$_A$
C5b (dbcot)	2.346(4)	2.211(3)	2.190(3)
C5f/1[b]	2.32(2)	2.17(2)	2.21(2)
C5f/2[b]	2.38(2)	2.21(2)	2.20(2)
C5c (dbcot)	2.397(4)	2.233(4)	2.204(4)
C5g/1[b]	2.413(8)	2.226(8)	2.168(8)
C5g/2[b]	2.452(9)	2.228(8)	2.173(8)

[a] The designations "/1" and "/2" refer to independent molecules within the unit cell. [b] **C5f** = [Ir(cod)(*C,P*-**L2**)(crotyl)]OTf, **C5g** = [Ir(cod)(*C,P*-**L2**)(cinnamyl)]SbF_6; for structural data, see ref. [11].

*Survey: The formation of (π-allyl)Ir complexes **C5** from complex **C3***: In our previous computational investigation of the Ir-catalyzed allylic substitution reaction, we showed that the most stable π-allyl complex would give rise to the experimentally observed enantiomer of the product. Only a part of the catalytic cycle, the reaction of the (π-allyl)Ir species with NH_3 as a model nucleophile, was addressed. However, equilibration within the (π-allyl)Ir manifold is slow, which typically manifests itself in substantial memory effects.[16] This suggests that the enantioselectivity of the reaction is pre-determined at the early stage of the *formation* of the allylic intermediate. In this scenario, the reaction of the 16 VE species **C3** with a chosen allylic substrate would result in the formation of the most stable, experimentally observed allylic complex. Accordingly, we computationally explored this pathway. Even if direct interconversion within the allylic manifold is slow, an indirect equilibration is possible if their formation by nucleophilic displacement is fast, reversible, and endergonic, as assumed by Hartwig and co-workers for allylic amination reactions. In that case, a Curtin–Hammett scenario would apply and the energy of the transition state of the reaction **C5**→**C6** would be the essential factor.

An *N,N,N*-trimethylcrotylammonium ion was chosen as the substrate that leads to the allylic manifold with the generation of a neutral leaving group to avoid complications associated with charge separation in the transition state, as would arise with commonly used anionic leaving groups. Experiments demonstrated that enantioselectivities comparable to those observed with the most commonly employed allylic carbonate substrates can be achieved (see above), thus justifying the choice of the model substrate.

First, we investigated the relative stability of all of the possible π-allyl complexes (**C5**, R = CH_3; Scheme 3) and then the oxidative addition step by calculating the energies of all of the transition states (**TS$_{Ox}$**, Scheme 2 and Scheme 5) leading to them. Then, the two pathways with the lowest values of the transition state energies were explored in full.

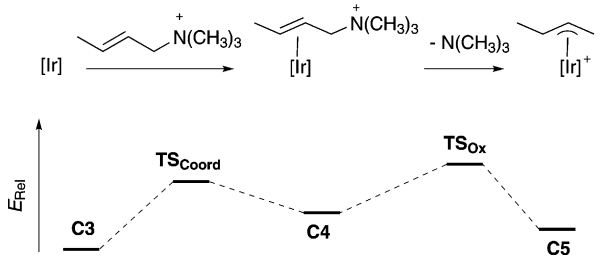

Scheme 5. Schematic representation of the key steps leading to the formation of complexes **C5** (R = CH_3).

*(π-Allyl)Ir complexes **C5** (R = CH_3, diene = dbcot, Ar = o-(H_3CO)C_6H_4)*: As we have shown previously for cod complexes, there are eight fundamental configurations (R = H) of the (π-allyl)Ir complexes of type **C5**;[11] these are schematically described in Figure 9. Our previous computations that covered all of these possible configurations were carried out for the simplified system described in Figure 10, which contained a cyclooctatetraene moiety and a chiral P,C ligand derived from 2,2′-dihydroxybiphenyl rather than BINOL. For this system, the P-series was favored over the C-series. This was mainly attributed to the fact that in the C-series the two ligands with the strongest *trans* influence, that is, the allyl ligand and the C8 atom of the chiral ligand (for atom numbering, see Figure 1), were located *trans* to each other.

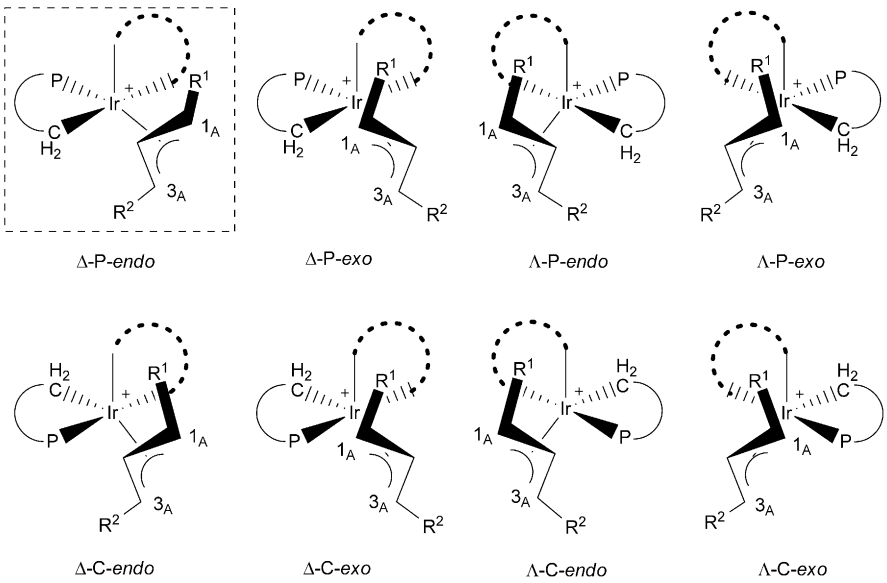

Figure 9. Schematic representations of the configurations of (π-allyl)Ir complexes **C5**; ·····= dbcot; P and C series: one of the allylic carbon atoms is located *trans* to the P atom and to the CH_2 group of the C,P ligand, respectively; *exo* and *endo*: the C2$_A$–H bond of the allyl ligand points towards dbcot and away from dbcot, respectively.

© 2012 Wiley-VCH Verlag GmbH & Co. KGaA, Weinheim

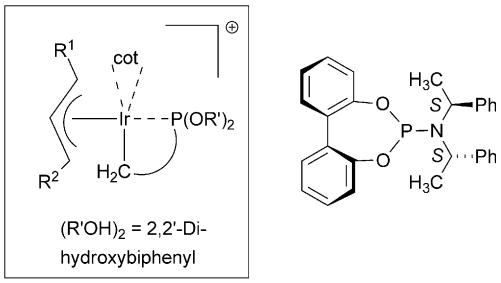

Figure 10. Previously used model for comparison of the relative energies of (π-allyl)Ir complexes (cot = cyclooctatetraene; see ref. [11a]).

No calculations had been done for complexes derived from the combination dbcot/**L2**. It was necessary to calculate the 16 nonsimplified allylic complexes **C5** ($R = CH_3$) in their lowest energy conformations (A/C, Figure 5) prior to investigating their formation. All of these calculations were done on conformer A, in which the two OCH_3 substituents adopted a *syn* disposition relative to the NC–H bonds (Figure 5). The crystallographically observed allylic complex Δ-P-*endo*-**C5** ($R^1 = H$, $R^2 = CH_3$) was computed to be the most stable isomer (Table 6). The corresponding complex was the most stable for the model system of Figure 10.

The experimentally observed isomer is energetically well separated from other structures. The next best calculated isomers, Δ-C-*endo*-**C5** ($R^1 = CH_3$, $R^2 = H$) and Δ-P-*endo*-**C5** ($R^1 = H$, $R^2 = CH_3$) were destabilized by 4 kcal mol^{-1} (Table 6, entries 5 and 9). The *endo* isomers are energetically preferred over their *exo* counterparts in the P-series, whereas, in the C-series, the difference is less pronounced. Other than previously found for the simplified model system, there is no clear energetic distinction between the P- and the C-series of the dbcot complexes. Although the lowest energy isomer has the P-configuration, the two next-best isomers ($R^1 = CH_3$ and $R^2 = H$) possess Δ-C-*endo*- (4.3 kcal mol^{-1}) and Δ-C-*exo* configurations (4.9 kcal mol^{-1}); these isomers are followed by Λ-P-*endo*-**C5** ($R^1 = CH_3$, $R^2 = H$; 5.1 kcal mol^{-1}). The difference between these dbcot complexes and the model system studied previously is most likely rooted in the higher steric requirement of the former system, so that the electronic effects are no longer dominant.

The crystallographically determined characteristic distances and angles were well reproduced by the calculations (Table 6, entry 1). The most pronounced deviation is observed for the Ir–$C1_A$ bond, which is substantially overestimated in the DFT calculations (2.44 Å vs. crystallographically determined 2.35 Å). For all structures with $R^1 = H$ and $R^2 = CH_3$, a more substantial distortion of the (π-allyl)Ir moiety into the direction of a η^1 structure is observed for the *exo* structures than for the *endo* structures (Table 6). The origin of this difference is likely the higher repulsion between the dbcot ligand and proton 2_A, which is oriented towards the dbcot ligand in the *exo* structures but not in the *endo* structures. However for $R^1 = H$ and $R^2 = CH_3$, both the Δ-P-*endo*- and Δ-P-*exo* isomers exhibit a weak tendency towards this distortion. As noted previously for the model system, the distortion is more pronounced in the C-series than in the P-series. Interestingly, within the C-series, the distortion is stronger for the *endo* complexes than for the *exo* complexes, which is opposite to the trend found in the P-series. In all cases, there is a preference for the isomer with $R^1 = CH_3$, $R^2 = H$ over the counterpart ($R^1 = H$, $R^2 = CH_3$).

Oxidative addition to afford allylic complexes ***C5*** *($R = CH_3$, $Ar = o\text{-}(H_3CO)C_6H_4$)*: All of the transition states of oxidative addition leading to the 16 π-allyl complexes **C5** ($R = CH_3$) were located (Figure 11); the results are presented in Table 7. A graphical representation of the lowest energy transition state is shown in Figure 14. The crystallographically observed and energetically favored (computation) allyl complex Δ-P-*endo*-**C5** ($R^1 = CH_3$, $R^2 = H$) was calculated to

Table 6. Relative energies [kcal mol^{-1}] and selected bond lengths [Å] and bond angles [°] of (π-allyl)Ir complexes **C5**; $R = CH_3$, diene = dbcot, $Ar = o\text{-}(H_3CO)C_6H_4$ (conformational isomers A, C; Figure 5).[a]

Entry	**C5**	Configuration	$E_{\mathbf{C5}}$[b]	Ir–$C1_A$	Ir–$C2_A$	Ir–$C3_A$	$C1_A$–$C2_A$	$C2_A$–$C3_A$	$C1_A$-$C2_A$-$C3_A$	P-Ir-CH_2
1	$R^1 = CH_3$, $R^2 = H$	Δ-P-*endo*	0	2.44	2.27	2.22	1.41	1.43	122.5	74.8
2	$R^1 = CH_3$, $R^2 = H$	Δ-P-*exo*	5.3	2.51	2.32	2.21	1.39	1.43	123.1	75.8
3	$R^1 = CH_3$, $R^2 = H$	Λ-P-*endo*	5.1	2.44	2.27	2.22	1.41	1.42	123.1	72.4
4	$R^1 = CH_3$, $R^2 = H$	Λ-P-*exo*	7.3	2.57	2.33	2.18	1.39	1.44	123.1	74.4
5	$R^1 = CH_3$, $R^2 = H$	Δ-C-*endo*	4.3	2.71	2.36	2.15	1.38	1.45	124.5	73.4
6	$R^1 = CH_3$, $R^2 = H$	Δ-C-*exo*	4.9	2.65	2.36	2.16	1.38	1.45	124.5	74.4
7	$R^1 = CH_3$, $R^2 = H$	Λ-C-*endo*	7.5	2.67	2.34	2.16	1.39	1.45	123.6	73.1
8	$R^1 = CH_3$, $R^2 = H$	Λ-C-*exo*	7.9	2.60	2.35	2.17	1.38	1.45	123.1	73.0
9	$R^1 = H$, $R^2 = CH_3$	Δ-P-*endo*	4.1	2.25	2.26	2.37	1.42	1.41	121.8	75.4
10	$R^1 = H$, $R^2 = CH_3$	Δ-P-*exo*	6.1	2.28	2.28	2.35	1.42	1.41	123.1	76.1
11	$R^1 = H$, $R^2 = CH_3$	Λ-P-*endo*	8.5	2.23	2.30	2.48	1.43	1.40	122.9	72.7
12	$R^1 = H$, $R^2 = CH_3$	Λ-P-*exo*	9.2	2.31	2.30	2.33	1.41	1.41	123.3	73.3
13	$R^1 = H$, $R^2 = CH_3$	Δ-C-*endo*	5.8	2.36	2.30	2.32	1.41	1.42	123.3	72.9
14	$R^1 = H$, $R^2 = CH_3$	Δ-C-*exo*	6.8	2.40	2.31	2.27	1.40	1.43	122.7	73.7
15	$R^1 = H$, $R^2 = CH_3$	Λ-C-*endo*	8.9	2.32	2.30	2.36	1.42	1.41	122.4	74.8
16	$R^1 = H$, $R^2 = CH_3$	Λ-C-*exo*	9.7	2.36	2.31	2.29	1.40	1.43	123.8	73.9

[a] All energies are normalized to the lowest energy allylic isomer **C5**, Δ-P-*endo* ($R^1 = CH_3$, $R^2 = H$). [b] Energies were obtained from solvent-corrected geometry optimizations (scrf-pcm, THF) with subsequent zero-point corrections.

© 2012 Wiley-VCH Verlag GmbH & Co. KGaA, Weinheim

These are not the final page numbers!

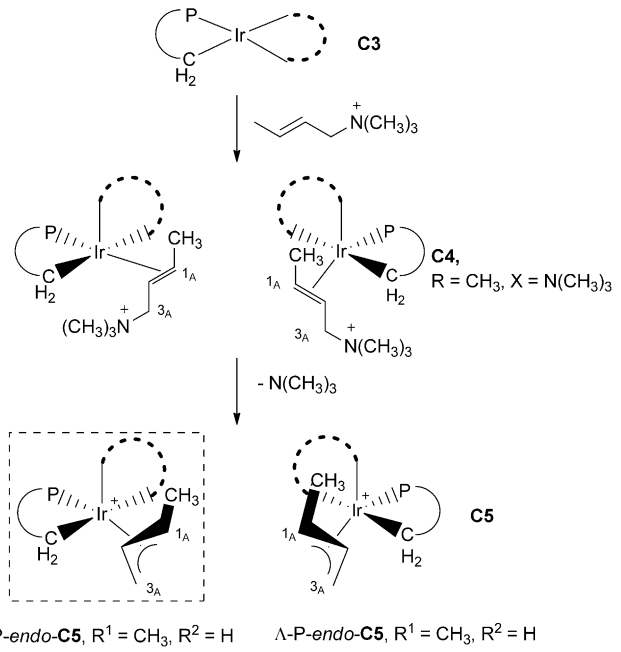

Figure 11. Pathways for the formation of the isomers of complex **C4** and isomers Δ-P-*endo*- and Λ-P-*endo*-**C5**, which are associated with the lowest and second lowest transition state energies ($\mathbf{TS_{Ox}}$), respectively; $R^1=CH_3$, $R^2=H$, diene = dbcot, Ar = *o*-$(H_3CO)C_6H_4$.

be associated with the lowest energy transition state for the oxidative addition step (Table 7, entry 1). In the following section, all other transition states ($\mathbf{TS_{Ox}}$) in the oxidative addition reaction are normalized to the lowest energy transition state.

The next-best reaction channel was determined computationally to be that of Λ-P-*endo*-**C5** ($R^1=CH_3$, $R^2=H$), with a relative transition-state energy of 2.1 kcal mol^{-1} (Table 7, entry 3), followed by five transition states with energies between 2.5 and 3.5 kcal mol^{-1}, all of which contained the substitution pattern $R^1=H$, $R^2=CH_3$. The next-best kinetic channel for an isomer with the substitution pattern $R^1=CH_3$, $R^2=H$ was calculated to be Δ-P-*exo*-**C5**. The transition-state energy was 2.7 kcal mol^{-1} higher than that computed for Λ-P-*endo*-**C5** ($R^1=CH_3$, $R^2=H$). Thus, these computational results are compatible with the view that the observed π-allyl complex is the most stable and also the kinetically preferred one.

The typical structural features of the transition states in the oxidative addition reaction can be summarized as follows: The length of the breaking C–N bond lies between 2.15 and 2.37 Å, thus spanning a rather broad range. The distance between iridium and the reacting carbon center adopts typical values between 2.70 and 2.98 Å.

Structure of complex ***C3*** *(diene = dbcot, Ar = o-$(H_3CO)C_6H_4$) and the possibilities for substrate coordination*: Having located the 16 transition states in the oxidative addition reaction, we proceeded to model the complete pathways for the formation of the two kinetically most viable isomers, Δ-P-*endo*- and Λ-P-*endo*-**C5** ($R^1=CH_3$, $R^2=H$), starting from the 16 VE complex **C3** (Figure 11).

A model of the d^8 16 VE complex **C3** was generated by removing the allylic moiety from the energetically lowest lying allylic complex, Δ-P-*endo*-**C5** ($R^1=H$, $R^2=CH_3$; Figure 9), followed by energy minimization of the residual fragment. As a control calculation, the same procedure was performed starting from Λ-P-*endo*-**C5** and Δ-C-*endo*-**C5** (both $R^1=H$, $R^2=CH_3$), which produced the same structure of complex **C3**. Complex **C3** was found to possess square-planar geometry with respect to the iridium center.

Table 7. Energies [kcal mol^{-1}] and selected bond lengths [Å] and torsion angles [°] of the transition states for the oxidative addition step ($\mathbf{TS_{Ox}}$, Scheme 5).

Entry	Descriptor	E_{TSox}	N–C3$_A$[a]	Ir–C1$_A$	Ir–C2$_A$	Ir–C3$_A$	C8-Ir-C2$_A$-C1$_A$	C8-Ir-C2$_A$-H2$_A$	Ir-C1$_A$-C2$_A$-C3$_A$
$R^1=CH_3$, $R^2=H$									
1	Δ-P-*endo*	0	2.20	2.27	2.28	2.74	−99.0	14.8	79.5
2	Δ-P-*exo*	4.8	2.31	2.28	2.30	2.77	−70.0	176.3	−80.5
3	Λ-P-*endo*	2.1	2.30	2.26	2.28	2.70	94.6	−19.5	−77.9
4	Λ-P-*exo*	6.5	2.37	2.27	2.34	2.79	65.0	178.2	79.4
5	Δ-C-*endo*	8.2	2.20	2.28	2.30	2.75	179.9	−66.6	79.1
6	Δ-C-*exo*	9.3	2.22	2.28	2.32	2.79	−146.6	100.9	−78.7
7	Λ-C-*endo*	13.4	2.26	2.27	2.32	2.77	−179.1	67.5	−79.5
8	Λ-C-*exo*	12.8	2.27	2.26	2.30	2.83	155.4	−90.2	84.2
Entry	Descriptor	E_{TSox}	N–C1$_A$	Ir–C1$_A$	Ir–C2$_A$	Ir–C3$_A$	C8-Ir-C2$_A$-C3$_A$	C8-Ir-C2$_A$-H2$_A$	Ir-C3$_A$-C2$_A$-C1$_A$
$R^1=H$, $R^2=CH_3$									
9	Δ-P-*endo*	3.0	2.19	2.78	2.28	2.25	123.0	10.6	−81.6
10	Δ-P-*exo*	2.5	2.27	2.78	2.30	2.21	79.7	−168.2	78.5
11	Λ-P-*endo*	7.0	2.26	2.77	2.28	2.25	−118.6	−6.3	80.6
12	Λ-P-*exo*	2.9	2.37	2.76	2.31	2.21	−84.4	163.4	−76.5
13	Δ-C-*endo*	3.5	2.16	2.89	2.31	2.20	42.3	−69.3	−84.5
14	Δ-C-*exo*	3.0	2.24	2.98	2.33	2.17	1.2	114.2	88.7
15	Λ-C-*endo*	8.2	2.15	2.94	2.31	2.19	−39.2	71.2	86.9
16	Λ-C-*exo*	8.8	2.21	2.98	2.33	2.18	−0.8	−115.0	−90.2

[a] The atom numbering of the allylic moiety depends on the way in which it is coordinated to the iridium atom. For the isomers with $R^1=H$ and $R^2=CH_3$, the relevant distance is N–C1$_A$. The same is true for dihedral angles C8-Ir-C2$_A$-C1$_A$ and Ir-C1$_A$-C2$_A$-C3$_A$.

© 2012 Wiley-VCH Verlag GmbH & Co. KGaA, Weinheim

Upon coordination of the olefinic substrate, the dbcot ligand has to rotate out of the plane to accommodate the steric bulk of the incoming allylic substrate and to enable constructive orbital overlap between the LUMO of the alkene (π^*) and the HOMO of complex **C3** (mainly d_{z^2} at the iridium atom). The relevant orbitals are shown in Figure 12. Notably, the substrate cannot approach complex

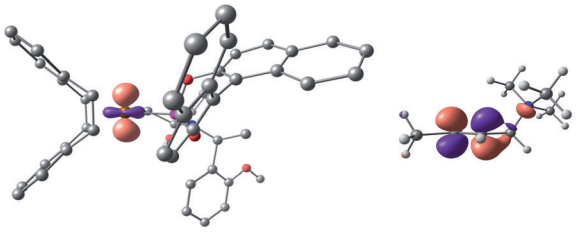

Figure 12. HOMO of complex **C3** (left) and LUMO of the allylic substrate (right); diene = dbcot, Ar = *o*-$(H_3CO)C_6H_4$.

C3 from above because this would not lead to constructive overlap between the HOMO of complex **C3** and the LUMO of the substrate. The possible trajectories of the substrate that do not violate orbital symmetry are shown in Figure 13.

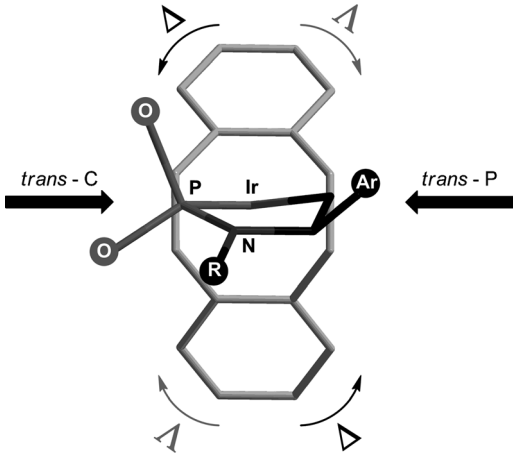

Figure 13. Possible structural adaptations of complex **C3**. The descriptors *trans*-C and *trans*-P designate the direction of the incoming substrate, whereas the curved arrows indicate the sense of rotation of dbcot, thereby generating the Δ or Λ chirality. For a color Figure see, the Supporting Information.

The Λ/Δ chirality at the iridium center, as well as the P/C configuration, are determined during the substrate coordination step, which gives rise to a total of the four possible coordination isomers (Δ-P, Λ-P, Δ-C, and Λ-C). The *exo*/*endo* configuration and the position of the methyl group relative to the rest of the coordination sphere of the iridium center ($C1_A$ or $C3_A$) are determined by the rotational state of the olefin within each of the coordination isomers.

The results for the reaction that proceeds from complex **C3** to allyl complexes **C5** are described in Table 8 and

Table 8. Energies [kcal mol^{-1}] of the species described in Figure 14.

Entry	Descriptor		E_{Rel}
1		**C3**	0.0
2	Δ-P-*endo*	$\mathbf{TS_{Coord}}$	13.0
3	$R^1=CH_3$, $R^2=H$	**C4**	5.3
4		$\mathbf{TS_{Ox}}$	14.5
5		**C5**	2.8
6	Λ-P-*endo*	$\mathbf{TS_{Coord}}$	9.8
7	$R^1=CH_3$, $R^2=H$	**C4**	4.3
8		$\mathbf{TS_{Ox}}$	16.6
9		**C5**	7.9

Figure 14. All of the stationary points are normalized to complex **C3**/substrate/NH_3. Starting from the isolated allylic substrate and complex **C3** (0.0 kcal mol^{-1}), olefin complexes **C4** are formed in an endergonic reaction (5.3 and 4.3 kcal mol^{-1} for configurations Δ-P-*endo* and Λ-P-*endo* ($R^1=CH_3$, $R^2=H$), respectively). The corresponding transition states ($\mathbf{TS_{Coord}}$) possess energies of 13.0 kcal mol^{-1} (Δ-P-*endo*) and 9.8 kcal mol^{-1} (Λ-P-*endo*), which are substantially lower than the subsequent barriers ($\mathbf{TS_{Ox}}$) of oxidative addition (14.5 and 16.6 kcal mol^{-1}, respectively). This identifies $\mathbf{TS_{Ox}}$ computationally as the rate-determining step for the formation of the allylic species, that is, the enantioselectivity of the reaction might be determined by the relative rates of formation of the allylic manifold. The geometric aspects of the formation of the allylic complexes are discussed in the Supporting Information.

*Reaction of Δ-P-endo-**C5** ($R^1=CH_3$, $R^2=H$, $Ar=o$-$(MeO)C_6H_4$) with NH_3 as the model nucleophile to yield complex **C6***: The reactivity of Δ-P-*endo*-**C5** in the allylic substitution reaction was assessed by conducting calculations with ammonia as the model nucleophile. The activation barriers were computed as 11.6 kcal mol^{-1} and 16.0 kcal mol^{-1} for the reactions at the $C1_A$ and $C3_A$ positions, respectively, thereby producing the corresponding olefin complexes **C6**. This mirrors well the experimentally observed regioselectivity of the reaction and agrees with our previous computational investigations. For the corresponding olefin complexes **C6**, energies of 0.5 kcal mol^{-1} (branched) and 2.6 kcal mol^{-1} (linear) were found relative to the state allyl complex/isolated NH_3.

The difference in activation energies for amination at the $C1_A$ (branched) versus $C3_A$ positions (linear) is 4.4 kcal mol^{-1}, which is essentially identical to the energetic difference for the analogous unsimplified cyclooctadiene-based system (4.3 kcal mol^{-1}), as previously reported by our group.[11a] However, whereas the relative order of stability of product complexes **C6** is marked for the dbcot complexes, it was small for the cod complexes (0.4 kcal mol^{-1}) and favored the linear product.

Conclusion

A very convenient one-pot procedure for the preparation of phosphoramidite-derived cyclometalated (π-allyl)Ir com-

© 2012 Wiley-VCH Verlag GmbH & Co. KGaA, Weinheim

These are not the final page numbers!

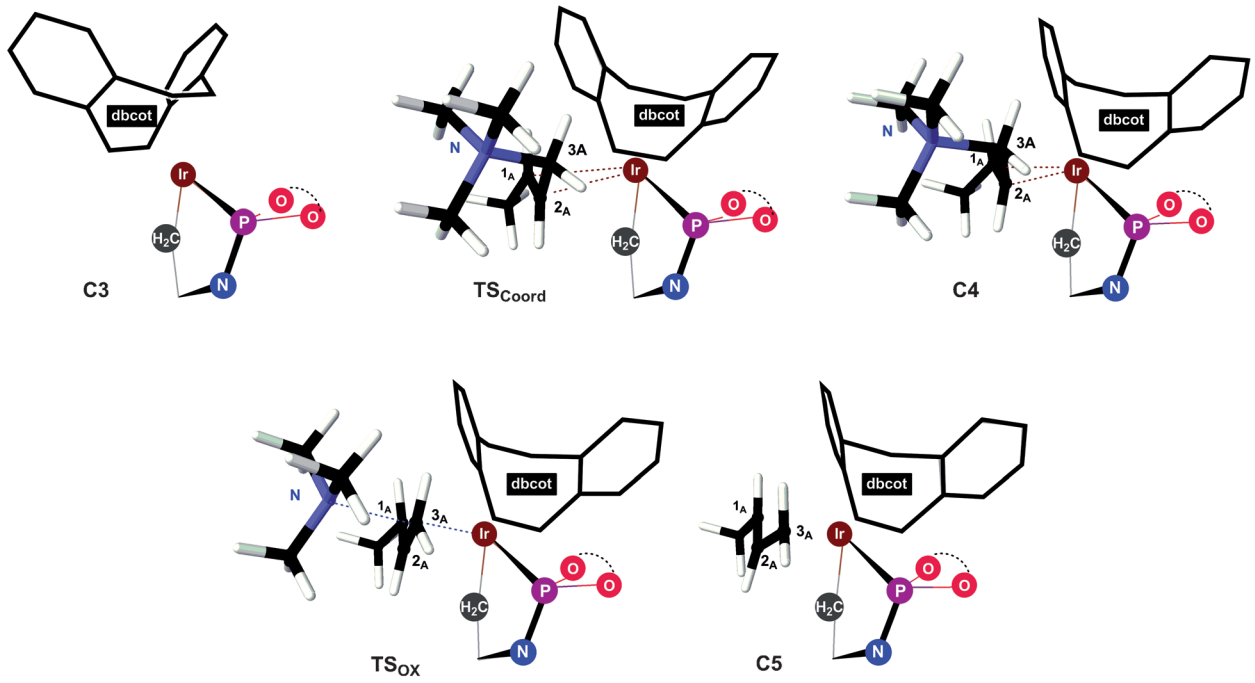

Figure 14. Relevant stationary points for the formation of allylic complex Δ-P-*endo*-**C5** from compound **C3**; $R^1 = CH_3$, $R^2 = H$, diene = dbcot, Ar = *o*-$(H_3CO)C_6H_4$.

plexes containing the ligand dbcot is described; the structures of the complexes were determined by X-ray crystal structure analysis. Allylic substitution reactions with dbcot complexes as single-species catalysts were found to generally proceed with a high degree of both regio- and enantioselectivity; a wide variety of solvents as well as aerobic conditions are tolerated. For an allylic amination reaction with aniline, the resting states were different for the reactions run with and without the presence of a strong base.

DFT calculations on nonsimplified models satisfactorily reproduced the structural and energetic features of the new (π-allyl)Ir complexes. The computational investigation also considered several steps in the putative catalytic cycle. These results are consistent with the view that the preferentially formed π-allyl complexes are both the most stable and the kinetically preferred complexes.

Experimental Section

Computational details: For all of the computations, the hybrid Becke functional (B3)[17] for electron exchange and the correlation functional of Lee, Yang, and Parr (LYP),[18] as implemented in the GAUSSIAN 09 software package, was used.[19] The SDD basis set with the associated Effective Core Potential was employed for iridium.[20] For other atoms, the 6-31G(d) level of theory was used.[21]

Transition states were located by using restricted geometry optimizations as follows: The distance between the nitrogen nucleophile and the reacting carbon atom was fixed at 2.0 Å for the reactions at atoms $C1_A$ or $C3_A$. The geometries were then fully optimized as saddle points of first order by employing the Berny algorithm.[22] To confirm the nature of the stationary points, frequency calculations were undertaken, which yielded zero imaginary frequencies for all allyl and olefin complexes. The transition states in the amination reactions possessed one imaginary frequency, which represented the vector of the C–N bond formation in all cases. Zero-point energy corrections were carried out for all computed energies. Furthermore, the influence of the solvent was taken into account by employing the polarized continuum model (PCM-SCRF) in all calculations[23] with THF ($\varepsilon = 7.6$) as the solvent.[24]

General methods: ^{1}H NMR spectroscopy: Bruker AC-300 (300.13 MHz), Bruker Avance 500 (500.13 MHz) or Bruker Avance 600 (600.13 MHz); RT; CD_2Cl_2, $CDCl_3$, or [D_8]THF; chemical shifts (δ) are reported relative to TMS or to residual undeuterated solvent ($CHCl_3$ in $CDCl_3$ at $\delta_H = 7.26$ ppm);[25] signal multiplicity: s (singlet), d (doublet), t (triplet), q (quartet), m (multiplet), dd (doublet of doublets), dt (doublet of triplets), ddd (doublet of doublet of doublets), bs (broad signal). ^{1}H NMR spectra of all new compounds are given in the Supporting Information. ^{13}C NMR spectroscopy: Bruker AC-300 (75.48 MHz), Bruker Avance 500 (125.76 MHz) or Bruker Avance 600 (150.90 MHz); RT; CD_2Cl_2, $CDCl_3$, or [D_8]THF; chemical shifts (δ) are reported relative to residual undeuterated solvent $CHCl_3$ ($\delta_C = 77.16$ ppm, central line of the triplet);[25] designation of the multiplicity for {^{1}H} spectra: s (singlet, quaternary C atom), d (doublet, CH group), t (triplet, CH_2 group), q (quartet, CH_3 group). ^{31}P NMR spectroscopy: Bruker DRX-250 (101.26 MHz), Bruker AC-300 (121.50 MHz), Bruker Avance 500 (202.46 MHz), or Bruker Avance 600 (242.94 MHz); RT; CD_2Cl_2, $CDCl_3$, or [D_8]THF; chemical shifts (δ) are reported relative to TMS in the ^{1}H NMR spectrum.[26] For compounds **C5a**–**C5e**, assignments were confirmed by H,H COSY, H,C COSY, TOCSY, HMBC, NOESY, and DEPT spectra; for atom numbering, see Figure 1. HRMS (ESI+): Bruker ApexQe FT-ICR mass spectrometer.

Flash column chromatography: silica gel (0.032–0.062) from Macherey, Nagel and Co. Dry THF was obtained from MBraun, MB SPS-800 solvent purification system. The hygroscopic base 1,5,7-triazabicyclo-[4.4.0]dec-5-ene (TBD) was stored in a desiccator over KOH and weighing was carried out quickly. Unless otherwise stated, reactions were carried out under an argon atmosphere in anhydrous conditions. IUPAC names were generated by the ACD/Labs 6.0 programm from Advanced Chemistry Development, Inc.

© 2012 Wiley-VCH Verlag GmbH & Co. KGaA, Weinheim

The syntheses, spectroscopic data, and the determination of the enantiomeric excess of the following compounds have already been reported: **1a**;[9b] **1b**;[28] **1c**;[27] **2a**, Nu = $CH(CO_2CH_3)_2$;[28] **2a**, Nu = $N(Boc)_2$;[12] **2a**, Nu = NHPh;[4] **2a**, Nu = NHBn;[4] **2b**, Nu = $CH(CO_2CH_3)_2$;[29] **2c**, Nu = $CH(CO_2CH_3)_2$.[28,11a]

General procedure for the preparation of (π-allyl)Ir complexes (GP1): In a flame-dried Schlenk tube under an argon atmosphere, complex **C1** was prepared by stirring a solution of [{Ir(dbcot)Cl}$_2$] (8.6 mg, 10 μmol) and ligand **L*** (20 μmol) in dry THF (0.5 mL, <30 μg water per mL THF, Karl–Fischer titration) at room temperature for 30 min. Then, allylic carbonate (40 μmol) and AgX (20 μmol) were added to the orange solution, thereby causing the formation of a white precipitate. The mixture was stirred at room temperature for the stated time. The white precipitate was removed by filtration through a pad of Celite and excess carbonate was removed by flash column chromatography on silica gel (CH_2Cl_2 then CH_2Cl_2/isopropanol, 97:3).

General procedure for the allylic substitution reactions (GP2, Scheme 1): In a dry Schlenk flask under an argon atmosphere, a solution of [{Ir(dbcot)Cl}$_2$] (2 mol%), ligand **L2** (4 mol%), and TBD (8 mol%; in situ procedure) or compound **C5** (4 mol%) in absolute THF (0.5 mL) was prepared and stirred at room temperature for 10 min; then, carbonate **1** (0.5 mmol), a pronucleophile (0.6 mmol), and, possibly, a base (8 mol%) were added and the conversion was monitored by TLC.

(2*E*)-*N*,*N*,*N*-Trimethyl-3-phenylprop-2-en-1-aminium trifluoromethanesulfonate (4): Trimethylamine (4.2 M in EtOH, 1.19 mL, 5.0 mmol) and cinnamyl bromide (985 mg, 5.00 mmol) were added to a solution of sodium triflate (860 mg, 5.00 mmol) in acetone (15 mL). The mixture was stirred at room temperature for 30 min, and the resultant precipitate was removed by filtration through a pad of Celite. The crude product was subjected to flash column chromatography on silica gel (CH_2Cl_2/CH_3OH, 9:1) to yield compound **4** (1.372 g, 84%) as a yellowish oil. ^{1}H NMR (300.19 MHz, CD_3OD): δ = 7.59–7.54 (m, 2H; 2×Ph), 7.42–7.32 (m, 3H; 3×Ph), 7.00 (d, J = 15.7 Hz, 1H; C*H*Ph), 6.44 (dt, J = 15.7, 7.7 Hz, 1H; C*H*CH_2), 4.11 (d, J = 7.6 Hz, 2H; CH_2), 3.15 ppm (s, 9H; CH_3); ^{13}C NMR (75.48 MHz, CD_3OD): δ = 144.47 (d; *C*HPh), 136.49 (s; Ph), 130.39 (d; Ph), 129.86 (d; 2×Ph), 128.37 (d; 2×Ph), 116.12 (d; *C*HCH_2), 69.46 (t; CH_2), 53.07 ppm (q; 3×CH_3); HRMS (ESI+): m/z calcd for $C_{25}H_{36}F_3N_2O_3S^+$: 501.23932; found: 501.23967 [$2M$+CF_3SO_3]$^+$.

C5a: According to GP1, [{Ir(dbcot)Cl}$_2$] (86 mg, 100 μmol) and ligand (*R*,*R*,a*R*)-**L2** (120 mg, 200 μmol) were stirred in dry THF (5 mL) at room temperature for 30 min. Allyl methyl carbonate (46.4 mg, 400 μmol) and AgOTf (51 mg, 200 μmol) were added. After 24 h, the resultant white precipitate was removed by filtration and the crude product was subjected to flash column chromatography on silica gel (CH_2Cl_2 then CH_2Cl_2/isopropanol, 97:3) to yield compound **C5a** (228 mg, 96%) as a light yellow powder. ^{1}H NMR (600.13 MHz, CD_2Cl_2): δ = 8.31 (d, J = 8.7 Hz, 1H; BINOL), 8.20 (d, J = 8.8 Hz, 1H; BINOL), 8.13 (d, J = 8.1 Hz, 1H; BINOL), 8.01 (d, J = 8.1 Hz, 1H; BINOL), 7.67 (d, J = 8.8 Hz, 1H; BINOL), 7.64 (d, J = 8.8 Hz, 1H; BINOL), 7.61 (dd, J = 7.4, 7.4 Hz, 1H; BINOL), 7.48–7.54 (m, 2H; BINOL, Ph), 7.41 (d, J = 7.4 Hz, 1H; Ph), 7.37 (dd, J = 7.7, 7.7 Hz, 1H; Ph), 7.33 (dd, J = 7.5, 7.5 Hz, 1H; Ph), 7.29 (dd, J = 7.3, 7.3 Hz, 1H; BINOL), 7.27 (dd, J = 7.3, 7.3 Hz; 1H; BINOL), 7.18–7.24 (m, 2H; BINOL, Ph), 7.03 (d, J = 7.6 Hz, 1H; Ar_{dbcot}), 6.96–7.01 (m, 3H; 2×Ph, Ar_{dbcot}), 6.89–6.94 (m, 3H; Ph, Ar_{dbcot}, BINOL), 6.82 (d, J = 7.5 Hz, 1H; Ar_{dbcot}), 6.77 (d, J = 7.7 Hz, 1H; Ar_{dbcot}), 6.48 (dd, J = 7.3, 7.3 Hz, 1H; Ar_{dbcot}), 6.04 (dd, J = 7.8, 7.8 Hz, 1H; 2_C-H), 5.68 (dd, J = 7.3, 7.3 Hz, 1H; Ar_{dbcot}), 5.13 (d, J = 8.2 Hz, 1H; 4_C-H), 5.10 (d, J = 7.5 Hz, 1H; Ar_{dbcot}), 4.76 (dd, J = 7.5, 7.5 Hz, 1H; 3_C-H), 4.68–4.73 (m, 1H; 7-H), 4.63–4.68 (m, 1H; 2_A-H), 4.51–4.56 (m, 1H; $1_{A,syn}$-H), 4.44–4.51 (m, 1H; 7′-H), 4.31 (d, J = 9.2 Hz, 1H; 1_C-H), 3.86 (s, 3H; OCH_3), 3.76 (dd, J = 10.3, 10.3 Hz, 1H; $1_{A,anti}$-H), 3.58 (s, 3H; OCH_3), 3.49 (dd, J = 7.9, 7.9 Hz, 1H; $3_{A,syn}$-H), 2.61 (d, J = 11.9 Hz, 1H; $3_{A,anti}$-H), 2.00 (dd, J = 11.6, 5.6 Hz, 1H; 8b-H), 0.90 (dd, J = 11.3, 11.3 Hz, 1H; 8a-H), 0.55 ppm (d, J = 7.4 Hz, 3H; 8′-H); ^{13}C{^{1}H} NMR (150.90 MHz, CD_2Cl_2): δ = 156.50, 156.39 (s; 2×Ph), 147.87 (s, J(C,P) = 16.5 Hz; BINOL), 146.12 (s, J(C,P) = 7.6 Hz; BINOL), 142.99, 140.66, 138.98, 136.71 (s; 4×Ar_{dbcot}), 132.83, 132.18, 131.71 (s; 3×BINOL), 131.47 (d; BINOL), 131.15 (s; BINOL), 130.96 (d; BINOL), 129.44 (s, J(C,P) = 11.6 Hz; Ph), 128.97, 128.70, 128.48, 128.27 (d; 4×Ph), 128.10, 128.01 (d; BINOL), 127.80, 127.25, 127.08 (d; 3×Ar_{dbcot}), 126.97 (d; BINOL), 126.70 (d; Ph), 126.70 (d; Ar_{dbcot}), 126.70, 126.59, 126.36 (d; 3×BINOL), 126.11 (d; Ar_{dbcot}), 125.93, 125.58 (d; 2×BINOL), 125.58, 124.81 (d; 2×Ar_{dbcot}), 123.94 (d; Ph), 121.36, 121.21 (s; 2×BINOL), 120.83 (d; BINOL), 120.53, 120.07 (d; 2×Ph), 119.86 (d; BINOL), 110.36 (d; Ph), 110.05 (d; Ar_{dbcot}), 106.80 (d; $C2_A$), 104.64 (d; $C1_C$), 93.62 (d; $C2_C$), 88.84 (d, J(C,P) = 4.4 Hz; $C3_C$), 75.51 (d, J(C,P) = 5.8 Hz; $C4_C$), 60.88 (t, J(C,P) = 29.3 Hz; $C1_A$), 59.45 (d, J(C,P) = 33.0 Hz; C7), 55.89 (t; $C3_A$), 55.98, 54.44 (q; 2×OCH_3), 51.98 (d, J(C,P) = 5.3 Hz; C7′), 22.15 (t, J(C,P) = 6.5 Hz; C8), 18.50 ppm (q; C8′); ^{31}P{^{1}H} NMR (242.94 MHz, CD_2Cl_2): δ = 111.61 ppm; HRMS (ESI+): m/z calcd for $C_{57}H_{50}IrNO_4P^+$: 1036.31057; found: 1036.30991 [M]$^+$.

C5b: According to GP1, [{Ir(dbcot)Cl}$_2$] (167 mg, 193 μmol) and ligand (*S*,*S*,a*S*)-**L2** (234 mg, 396 μmol) were stirred in dry THF (10 mL) at room temperature for 30 min. Then, crotyl methyl carbonate (104 mg, 800 μmol) and AgOTf (103 mg, 400 μmol) were added. After 18 h, the resultant white precipitate was removed by filtration and the crude product was subjected to flash column chromatography on silica gel (CH_2Cl_2 then CH_2Cl_2/isopropanol, 97:3) to yield compound **C5b** (457 mg, 98%) as a light yellow powder. ^{1}H NMR (500.13 MHz, CD_2Cl_2): δ = 8.28 (d, J = 8.7 Hz, 1H; BINOL), 8.19 (d, J = 8.8 Hz, 1H; BINOL), 8.13 (d, J = 8.2 Hz, 1H; BINOL), 8.01 (d, J = 8.1 Hz, 1H; BINOL), 7.59–7.66 (m, 3H; 3×BINOL), 7.46–7.55 (m, 3H; 2×Ph, BINOL), 7.26–40 (m, 4H; 2×Ph, 2×BINOL), 7.157.23 (m, 2H; Ph, BINOL), 6.88–7.07 (m, 7H; 3×Ph, BINOL, 3×Ar_{dbcot}), 6.78 (d, J = 7.5 Hz, 1H; Ar_{dbcot}), 6.75 (d, J = 7.4 Hz, 1H; Ar_{dbcot}), 6.47 (dd, J = 7.2, 7.2 Hz, 1H; Ar_{dbcot}), 5.99 (dd, J = 7.6, 7.6 Hz, 1H; $dbcot_{ol}$-H), 5.67 (dd, J = 7.3, 7.3 Hz, 1H; Ar_{dbcot}), 5.12 (d, J = 7.4 Hz, 1H; Ar_{dbcot}), 4.71 (dd, J = 6.8, 6.8 Hz, 1H; $dbcot_{ol}$-H), 4.42–4.59 (m, 4H; 7-H, 7′-H, 1_A-H, 2_A-H), 4.19–4.24 (m, 1H; $dbcot_{ol}$-H), 4.13 (d, J = 9.1 Hz, 1H; $dbcot_{ol}$-H), 3.8 (s, 3H; OCH_3), 3.54 (s, 3H; OCH_3), 3.02 (m, 1H; $3_{A,syn}$-H), 2.36 (dd, J = 11.6, 4.6 Hz, 1H; 8b-H), 2.09–2.16 (m, 1H; $3_{A,anti}$-H), 1.70–1.76 (m, 3H; CH_3), 0.80 (dd, J = 11.9, 11.9 Hz, 1H; 8a-H), 0.56 ppm (d, J = 7.3 Hz, 3H; 8′-H); ^{13}C{^{1}H, ^{31}P} NMR (125.76 MHz, CD_2Cl_2): δ = 156.53, 156.46 (s; 2×Ar), 147.83, 146.15 (s; 2×BINOL), 142.62, 141.32, 139.24, 136.66 (s; 4×Ar_{dbcot}), 132.9, 132.25, 131.75 (s; 3×BINOL), 131.44 (d; BINOL), 131.26 (s; BINOL), 130.97 (d; BINOL), 129.60 (s; Ar), 129.10 (d; Ar), 128.71 (d; Ar), 128.51 (s; Ar), 128.20 (d; Ar), 128.15 (d; BINOL), 128.03 (d; BINOL), 127.57 (d; Ar_{dbcot}), 127.11, 127.07, 126.98, 126.93, 126.87, 126.75, 126.71, 126.66, 126.39 (d; 9×Ar), 125.99 (d; BINOL), 125.64 (d; Ar_{dbcot}), 125.49 (d; BINOL), 124.81 (d; Ar_{dbcot}), 123.62 (d; Ar), 121.44, 120.86 (s; 2×BINOL), 120.67, 120.15, 119.97 (d; 3×Ar), 110.36 (d; Ar_{dbcot}), 110.10 (d; Ar), 107.00 (d; $C2_A$), 103.81 (d; CH-$dbcot_{ol}$), 93.82 (d; CH-$dbcot_{ol}$), 91.27 (d; CH-$dbcot_{ol}$), 84.46 (d; $C1_A$), 81.67 (d; CH-$dbcot_{ol}$), 59.10 (d; C7), 54.99, 54.43 (q; 2×OCH_3), 51.77 (d; C7′), 47.97 (t; $C3_A$), 18.44 (q; C8′), 18.08 (t; C8), 14.61 ppm (q; CH_3); ^{31}P{^{1}H} NMR (202.47 MHz, CD_2Cl_2): δ = 112.92 ppm; HRMS (ESI+): m/z calcd for $C_{58}H_{52}IrNO_4P^+$: 1050.32623; found: 1050.32467 [M]$^+$.

C5c: According to GP1, [{Ir(dbcot)Cl}$_2$] (173 mg, 200 μmol) and ligand (*R*,*R*,a*R*)-**L2** (240 mg, 400 μmol) were stirred in dry THF (10 mL) at room temperature for 30 min. Then, cinnamyl methyl carbonate **1a** (154 mg, 800 μmol) and AgOTf (103 mg, 400 μmol) were added. After 18 h, the resultant white precipitate was removed by filtration and the crude product was subjected to flash column chromatography on silica gel (CH_2Cl_2 then CH_2Cl_2/isopropanol, 97:3) to yield compound **C5c** (478 mg, 95%) as a light yellow powder. ^{1}H NMR (600.13 MHz, CD_2Cl_2): δ = 8.33 (d, J = 8.8 Hz, 1H; BINOL), 8.20 (d, J = 8.9 Hz, 1H; BINOL), 8.15 (d, J = 8.2 Hz, 1H; BINOL), 8.01 (d, J = 8.4 Hz, 1H; BINOL), 7.71 (d, J = 8.8 Hz, 1H; BINOL), 7.60–7.66 (m, 2H; 2×BINOL), 7.57 (d, J = 7.9 Hz, 1H; Ph), 7.48–7.53 (m, 2H; Ph, BINOL), 7.35–7.41 (m, 3H; Ph_{Allyl}, 2×Ph), 7.20–7.32 (m, 5H; 2×Ph_{Allyl}, 3×BINOL), 7.18 (dd, J = 7.3, 7.3 Hz, 1H; Ph), 7.04–7.10 (m, 3H; Ar_{dbcot}, 2×Ph), 6.98 (ddd, J = 7.6, 7.6, 1.1 Hz, 1H; Ar_{dbcot}), 6.95 (d, J = 8.0 Hz, 1H; Ph), 6.91 (d, J = 8.5 Hz, 1H; BINOL), 6.89 (d, J = 7.7 Hz, 1H; Ar_{dbcot}), 6.76–6.83 (m, 2H; 2×Ph_{Allyl}), 6.69 (d, J = 7.6 Hz, 1H; Ar_{dbcot}), 6.67 (d, J = 7.7 Hz, 1H; Ar_{dbcot}), 6.45 (dd, J = 7.3, 7.3 Hz, 1H; Ar_{dbcot}), 6.10 (dd, J = 9.0, 6.5 Hz, 1H; $dbcot_{ol}$-H), 5.65 (dd, J = 7.4, 7.4 Hz, 1H; Ar_{dbcot}), 5.43–5.50 (m, 1H; 1_A-H), 5.23–5.30 (m, 1H; 2_A-H), 5.18 (d, J = 7.7 Hz, 1H; Ar_{dbcot}), 4.71 (dd, J = 11.8, 5.3 Hz, 1H; 7-H), 4.53–4.64 (m, 2H; 7′-H, $dbcot_{ol}$-H), 4.47 (d, J = 9.1 Hz, 1H;

© 2012 Wiley-VCH Verlag GmbH & Co. KGaA, Weinheim

These are not the final page numbers!

dbcot$_{ol}$-H), 4.10 (s, 3H; OCH_3), 3.59 (s, 3H; OCH_3), 3.46 (dd, J=8.7, 3.2 Hz, 1H; dbcot$_{ol}$), 3.05 (dd, J=7.5, 7.5 Hz, 1H; $3_{A,syn}$-H), 2.27–2.34 (m, 2H; 8b-H, $3_{A,anti}$-H), 0.80 (dd, J=11.7, 11.7 Hz, 1H; 8a-H), 0.59 (d, J=7.5 Hz, 3H; 8′-H); $^{13}C\{^1H\}$ NMR (150.90 MHz, CD_2Cl_2): δ=156.55, 156.29 (s; 2×Ph), 147.72 (s, J(C,P)=16.6 Hz; BINOL), 146.05 (s, J-(C,P)=8.5 Hz; BINOL), 141.49, 141.45, 139.36, 137.14 (s; 4×Ar$_{dbcot}$), 132.85, 132.23 (s; 2×BINOL), 132.07 (s, J(C,P)=6.0 Hz; Ph$_{Allyl}$), 131.79 (s; BINOL), 131.52 (d; BINOL), 131.27 (s; BINOL), 131.00 (d; BINOL), 129.63 (d; Ar$_{dbcot}$), 129.52 (s, J(C,P)=12.8 Hz; Ph), 129.36, 129.26, 128.82 (d; 3×Ph), 128.40, 128.39 (d; 2×Ph$_{Allyl}$), 128.35 (s; Ph), 128.21 (d; Ph), 128.14, 128.05 (d; 2×BINOL), 127.21 (2d; 2×Ph$_{Allyl}$), 127.10 (d; Ar$_{dbcot}$), 127.08 (d; Ph), 126.94 (d; BINOL), 126.83 (d; Ar$_{dbcot}$), 126.83, 126.71 (d; 2×BINOL), 126.71 (d; Ar$_{dbcot}$), 126.42 (d; Ph), 126.32 (d; Ar$_{dbcot}$), 126.06 (d; BINOL), 125.71 (d; Ar), 125.51, 124.89 (d; 2×Ar$_{dbcot}$), 123.40 (d; Ph), 121.45, 121.42 (s; 2×BINOL), 120.83 (d; BINOL), 120.83, 120.28 (d; 2×Ph), 119.82 (d; BINOL), 110.21 (d; Ar$_{dbcot}$), 110.16 (d; Ph), 102.95 (d; CH-dbcot$_{ol}$), 97.66 (d, J(C,P)=4.0 Hz; C2$_A$), 93.37 (d, J(C,P)=4.6 Hz; CH-dbcot$_{ol}$), 93.15 (d; CH-dbcot$_{ol}$), 90.26 (d, J(C,P)=22.6 Hz; C1$_A$), 84.77 (d, J(C,P)=6.6 Hz; CH-dbcot$_{ol}$), 59.17 (d, J(C,P)=31.2 Hz; C7), 54.90, 54.51 (q; 2×OCH_3), 51.77 (d, J(C,P)=4.8 Hz; C7′),46.01 (t; C3$_A$), 21.55 (t, J(C,P)=7.7 Hz; C8), 18.40 (q; C8′); $^{31}P\{^1H\}$ NMR (242.94 MHz, CD_2Cl_2): δ=110.81 ppm; HRMS (ESI+): m/z calcd for $C_{63}H_{54}IrNO_4P^+$: 1112.34195; found: 1112.34094 $[M]^+$.

C5d: According to GP1, [{Ir(dbcot)Cl}$_2$] (173 mg, 201 μmol) and ligand (*S*,*S*,a*S*)-**L1** (217 mg, 402 μmol) were stirred in dry THF (10 mL) at room temperature for 60 min. Then, crotyl methyl carbonate (104 mg, 798 μmol) and AgOTf (104 mg, 406 μmol) were added. After 21 h, the resultant white precipitate was removed by filtration and the crude product was subjected to flash column chromatography on silica gel (CH_2Cl_2 then CH_2Cl_2/isopropanol, 97:3) to yield compound **C5d** (385 mg, 84%) as a light-yellow powder. ^1H NMR (500.13 MHz, CD_2Cl_2): δ=8.35 (d, J=8.8 Hz, 1H; BINOL), 8.16 (2d, J=8.7 Hz, 2H; 2×BINOL), 7.98 (d, J=8.2 Hz, 1H; BINOL), 7.76 (d, J=8.8 Hz, 1H; BINOL), 7.61–7.66 (m 2H; 2×BINOL), 7.47–7.53 (m, 3H; BINOL, 2×Ph), 7.26–7.43 (m 8H; 2×BINOL, 6×Ph), 7.17–7.23 (m, 3H; BINOL, 2×Ph), 7.06 (d, J=7.5 Hz, 1H; Ar$_{dbcot}$), 6.92–7.01 (m, 3H; BINOL, 2×Ar$_{dbcot}$), 6.89 (d, J=7.6 Hz, 1H; Ar$_{dbcot}$), 6.76 (d, J=7.0 Hz, 1H; Ar$_{dbcot}$), 6.57 (dd, J=7.2, 7.2 Hz, 1H; Ar$_{dbcot}$), 5.87 (dd, J=8.9, 6.8 Hz, 1H; dbcot$_{ol}$-H), 5.82 (dd, J=7.2, 7.2 Hz, 1H; Ar$_{dbcot}$), 4.97 (d, J=7.6 Hz, 1H; Ar$_{dbcot}$), 4.85 (dd, J=8.5, 6.3 Hz, 1H; dbcot$_{ol}$-H), 4.38–4.52 (m, 2H; 2$_A$-H, 1$_A$-H), 4.27 (d, J=9.2 Hz, 1H; dbcot$_{ol}$-H), 4.22 (dd, J=8.6, 3.0 Hz, 1H; dbcot$_{ol}$-H), 3.89–3.98 (m, 1H; 7′-H), 3.81 (dd, J=11.5, 5.4 Hz, 1H; 7-H), 3.17–3.23 (m, 1H; $3_{A,syn}$-H), 2.38 (d, J=11.0 Hz, 1H; $3_{A,anti}$-H), 2.13 (dd, J=11.7, 5.6 Hz, 1H; 8b-H), 1.67 (dd, J=8.5, 5.3 Hz, 3H; CH_3), 1.04 (dd, J=11.6 Hz, 1H; 8a-H), 0.66 ppm (d, J=7.4 Hz, 3H; 8′-H); ^{13}C NMR (125.76 MHz, CD_2Cl_2): δ=147.89 (s, J(C,P)=16.9 Hz; BINOL), 146.37 (s, J(C,P)=8.2 Hz; BINOL), 142.42 (s; Ar$_{dbcot}$), 141.22 (s, J(C,P)=10.6 Hz; Ph), 141.16 (s; Ar$_{dbcot}$), 139.73 (s; Ph), 139.05, 136.50 (s; 2×Ar$_{dbcot}$), 133.02, 132.22, 131.76 (s; 3×BINOL), 131.70 (d; BINOL), 131.21 (s; BINOL), 131.13 (d; BINOL), 129.07 (d; 2×Ph), 128.00, 128.06, 128.12, 128.14, 128.26, 128.26 (d; 2×BINOL, 4×Ph), 127.69 (d; 2×Ph), 127.51, 127.20 (d; 2×Ar$_{dbcot}$), 126.88, 126.94, 126.99, 127.12, 127.15 (d; BINOL, 4×Ar$_{dbcot}$), 126.78, 126.77, 126.42, 126.13 (d; 4×BINOL), 125.97 (d; 2×Ph), 125.78 (d; Ar$_{dbcot}$), 125.68 (d; BINOL), 125.04 (d; Ar$_{dbcot}$), 121.54 (s, J(C,P)=2.0 Hz; BINOL), 121.14 (s; BINOL), 120.95 (d, J(C,P)=3.3 Hz; BINOL), 119.70 (d; BINOL), 106.95 (d, J(C,P)=3.7 Hz; C2$_A$), 105.01 (d, J(C,P)=2.8 Hz; CH-dbcot$_{ol}$), 90.90 (d, J(C,P)=5.1 Hz; CH-dbcot$_{ol}$), 85.17 (d, J(C,P)=25.6 Hz; C1$_A$), 81.49 (d, J(C,P)=7.4 Hz; CH-dbcot$_{ol}$), 65.36 (d, J(C,P)=32.0 Hz; C7), 59.73 (d, J(C,P)=5.3 Hz; C7′), 48.21 (t; C3$_A$), 20.82 (t, J(C,P)=6.2 Hz; C8), 18.43 (q; C8′), 14.44 ppm (q, J-(C,P)=4.2 Hz; CH_3); $^{31}P\{^1H\}$ NMR (202.47 MHz, CD_2Cl_2): δ=112.68 ppm; HRMS (ESI+): m/z calcd for $C_{56}H_{48}IrNO_2P^+$: 990.30507; found 990.30502 $[M]^+$.

C5e: According to GP1, [{Ir(dbcot)Cl}$_2$] (86 mg, 100 μmol) and ligand (*S*,*S*,a*S*)-**L1** (108 mg, 200 μmol) were stirred in dry THF (5 mL) at room temperature for 60 min. Cinnamyl methyl carbonate **1a** (77 mg, 400 μmol) and AgOTf (51.4 mg, 200 μmol) were added. After 24 h, the resultant white precipitate was removed by filtration and the crude product was subjected to flash column chromatography on silica gel (CH_2Cl_2 then CH_2Cl_2/isopropanol, 97:3) to yield compound **C5e** (229 mg, 95%) as a light yellow powder. ^1H NMR (500.13 MHz, CD_2Cl_2): δ=8.37 (d, J=8.8 Hz 1H; BINOL), 8.15–8.21 (m, 2H; 2×BINOL), 7.99 (d, J=8.2 Hz, 1H; BINOL), 7.84 (d, J=8.8 Hz, 1H; BINOL), 7.62–7.67 (m, 2H; 2×BINOL), 7.48–7.57 (m, 3H; BINOL, 2×Ph), 7.27–7.47 (m, 9H; Ph$_{Allyl}$, 2×BINOL, 6×Ph), 7.20–7.27 (m, 5H; BINOL, 2×Ph$_{Allyl}$, 2×Ph), 7.06 (dd, J=7.3, 7.3 Hz, 1H; Ar$_{dbcot}$), 6.98 (dd, J=7.2, 7.2 Hz, 1H; Ar$_{dbcot}$), 6.94 (d, J=8.4 Hz, 1H; BINOL), 6.91 (d, J=7.7 Hz, 1H; Ar$_{dbcot}$), 6.81 (d, J=7.7 Hz, 1H; Ar$_{dbcot}$), 6.68–6.75 (m, 3H; Ar$_{dbcot}$, 2×Ph$_{Allyl}$), 6.54 (dd, J=7.4, 7.4 Hz, 1H; Ar$_{dbcot}$), 5.99 (d, J=9.3 Hz, 1H; dbcot$_{ol}$-H), 5.80 (dd, J=7.5, 7.5 Hz, 1H; Aryl$_{dbcot}$), 5.55 (d, J=13.0 Hz, 1H; 1$_A$-H), 5.14–5.23 (m, 1H; 2$_A$-H), 5.06 (d, J=7.7 Hz, 1H; Ar$_{dbcot}$), 4.79 (d, J=8.7 Hz, 1H; dbcot$_{ol}$-H), 4.64 (d, J=9.3 Hz, 1H; dbcot$_{ol}$-H), 3.91–4.07 (m, 2H; 7-H, 7′-H), 3.51 (d, J=8.7 Hz, 1H; dbcot$_{ol}$-H), 3.27 (d, J=6.8 Hz, 1H; $3_{A,syn}$-H), 2.60 (d, J=11.2 Hz, 1H; $3_{A,anti}$-H), 2.07 (dd, J=12.4, 5.4 Hz, 1H; 8b-H), 1.04 (dd, J=12.0 Hz, 1H; 8a-H), 0.69 ppm (d, J=7.4 Hz, 3H; 8′-H); ^{13}C NMR (125.76 MHz, CD_2Cl_2): 147.82 (s, J(C,P)=17.0 Hz; BINOL), 146.34 (s, J-(C,P)=8.8 Hz; BINOL), 141.44, 141.43, 141.39, 141.28, 139.73, 139.30, 137.19 (s; Ph$_{Allyl}$, 2×Ph, 4×Ar$_{dbcot}$), 132.96, 132.22, 131.86 (s; 3×BINOL), 131.81 (d; BINOL), 131.24 (s; BINOL), 131.17 (d; BINOL), 129.52, 129.66 (d; 2×Ph$_{Allyl}$), 129.10 (d; 2×Ph), 128.57 (d; 2×Ph$_{Allyl}$), 128.29 (d; 2×Ph), 128.15, 128.13 (d; BINOL), 127.87, 127.94, 127.79 (d; 4×Ph), 127.07, 127.09, 127.12, 127.18, 127.19 (d, BINOL; 3×Ar$_{dbcot}$, Ph$_{Allyl}$), 126.90, 126.81 (d; Ar$_{dbcot}$,), 126.77, 126.75, 126.41 (d; 3×BINOL), 126.35 (d; Ar$_{dbcot}$,), 126.11 (d; BINOL), 125.85 (d; 2×Ph), 125.74 (d; BINOL), 125.69, 125.12 (d; 2×Ar$_{dbcot}$), 121.46 (s; BINOL), 121.18 (s, J(C,P)=3.1 Hz; BINOL), 121.02 (d, J(C,P)=3.1 Hz; BINOL), 119.69 (d; BINOL), 104.14 (d; CH-dbcot$_{ol}$), 98.05 (d, J(C,P)=4.1 Hz; C2$_A$), 93.01 (d, J(C,P)=4.5 Hz; CH-dbcot$_{ol}$), 91.00 (d, J(C,P)=22.1 Hz; C1$_A$), 84.58 (d, J(C,P)=6.7 Hz; CH-dbcot$_{ol}$), 65.43 (d, J(C,P)=31.0 Hz; C7), 59.79 (d, J(C,P)=5.3 Hz; C7′),46.43 (t; C3$_A$), 24.18 (t, J(C,P)=6.4 Hz; C8), 18.37 ppm (q; C8′); $^{31}P\{^1H\}$ NMR (202.46 MHz, CD_2Cl_2): δ=110.57 ppm; HRMS (ESI+): m/z calcd for $C_{61}H_{50}IrNO_2P^+$: 1052.32079; found 1052.31884 $[M]^+$.

X-ray crystal structure analysis: Data sets were collected on a Bruker Smart CCD (**C5c**, **C5d**) or a Bruker APEX (**C5a**, **C5b**, **C5e**) diffractometer with $Mo_{K\alpha}$ radiation (l=0.71073 Å, graphite monochromator) at 200 K. A complete sphere in reciprocal space was covered by 0.3° w-scans in all cases. For all datasets, the intensities were corrected for Lorentz and polarization effects; an empirical absorption correction, based on the Laue symmetry of the reciprocal space, was applied by using SADABS.[30] All structures were solved by using direct methods and refined against $F2$ with a full-matrix least-squares algorithm and the SHELXTL software package.[31] Hydrogen atoms were treated by using appropriate riding models.

For compounds **C5a**, **C5b**, **C5c**, and **C5e**, the diffusion-controlled crystallization of racemates, which were obtained by mixing enantiomers, was performed as follows: In a shortened NMR tube (length 10 cm), a solution of racemic complex **C5** in CH_2Cl_2 was carefully covered with a layer of Et_2O. This procedure furnished crystals that were suitable for X-ray analysis. In the case of compound **C5d**, single crystals were obtained from a solution of the enantiopure compound, which was derived from ligand (*S*,*S*,a*S*)-**L1**, in [D_8]THF.

C5a: Brownish crystals (polyhedra); 0.28×0.14×0.10 mm^3; monoclinic; space group $C2/c$; Z=8; a=25.955(3), b=19.1317(19), c=21.760(2) Å; β=102.424(2)°; V=10552.2(18) Å^3; ρ=1.546 g cm^{-3}; θ_{max}=28.33°; total reflns 55471; unique reflns 13134 (R_{int}=0.0454); observed reflns 11057 [$I>2\sigma(I)$]; μ=2.72 mm^{-1}; T_{min}=0.52, T_{max}=0.77; 709 parameters refined; GOF 1.17 for observed reflections; final residual values $R1(F)$=0.056, $wR(F^2)$=0.137 for observed reflections; residual electron density −2.12 to 1.69 e Å^{-3}.

C5b: Brownish crystals (polyhedra); 0.22×0.22×0.14 mm^3; monoclinic; space group $C2/c$; Z=8; a=25.955(4), b=19.068(3), c=21.794(3) Å; β=102.170(3)°; V=10544(2) Å^3; ρ=1.564 g cm^{-3}; θ_{max}=28.39°; total reflns 55579; unique reflns 13169 (R_{int}=0.0352); observed reflns 11403 [$I>2\sigma(I)$]; μ=2.72 mm^{-1}; T_{min}=0.59, T_{max}=0.70; 698 parameters refined; GOF 1.08 for observed reflections; final residual values $R1(F)$=0.037,

 © 2012 Wiley-VCH Verlag GmbH & Co. KGaA, Weinheim

$wR(F^2)=0.091$ for observed reflections; residual electron density −0.66 to 1.92 e Å^{-3}.

C5c: Brownish crystals (polyhedra); $0.34\times0.22\times0.14$ mm^3; triclinic; space group $P\bar{1}$; $Z=2$; $a=12.1337(1)$, $b=14.9512(1)$, $c=18.4822(1)$ Å; $\alpha=85.5960(10)°$, $\beta=80.7790(10)°$, $\gamma=75.0460(10)°$; $V=3195.30(4)$ Å^3; $\rho=1.488$ g cm^{-3}; $\theta_{max}=27.47°$; total reflns 32222; unique reflns 14474 ($R_{int}=0.0406$); observed reflns 13031 [$I>2\sigma(I)$]; $\mu=2.38$ mm^{-1}; $T_{min}=0.50$, $T_{max}=0.73$; 853 parameters refined; GOF 1.08 for observed reflections; final residual values $R1(F)=0.040$, $wR(F^2)=0.105$ for observed reflections; residual electron density −1.39 to 1.64 e Å^{-3}.

C5d: Colorless crystals (polyhedra); $0.34\times0.27\times0.18$ mm^3; monoclinic; space group $P2_1$; $Z=2$; $a=13.8110(1)$, $b=11.5716(1)$, $c=17.0108(1)$ Å; $\beta=95.170(1)°$; $V=2707.53(3)$ Å^3; $\rho=1.471$ g cm^{-3}; $\theta_{max}=27.43°$; total reflns 27177; unique reflns 12047 ($R_{int}=0.0324$); observed reflns 11251 [$I>2\sigma(I)$]; $\mu=2.59$ mm^{-1}; $T_{min}=0.47$, $T_{max}=0.65$; 655 parameters refined; GOF 1.07 for observed reflections; final residual values $R1(F)=0.024$, $wR(F^2)=0.059$ for observed reflections; residual electron density −0.49 to 0.62 e Å^{-3}.

C5e: Brownish crystals (plates); $0.27\times0.24\times0.07$ mm^3; triclinic; space group $P\bar{1}$; $Z=4$; $a=16.0194(17)$, $b=16.9075(18)$, $c=23.284(3)$ Å; $\alpha=74.654(2)°$, $\beta=73.921(2)°$, $\gamma=68.160(2)°$; $V=5531.6(10)$ Å^3; $\rho=1.538$ g cm^{-3}; $\theta_{max}=28.49°$; total reflns 74653; unique reflns 27190 ($R_{int}=0.0416$); observed reflns 32494 [$I>2\sigma(I)$]; $\mu=2.59$ mm^{-1}; $T_{min}=0.54$, $T_{max}=0.84$; 1432 parameters refined; GOF 1.09 for observed reflections; final residual values $R1(F)=0.052$, $wR(F^2)=0.116$ for observed reflections; residual electron density −1.41 to 2.12 e Å^{-3}.

CCDC-883814 (**C5a**), CCDC-883815 (**C5b**), CCDC-883816 (**C5c**), CCDC-883817 (**C5d**), and CCDC-883818 (**C5e**) contain the supplementary crystallographic data for this paper. These data can be obtained free of charge from The Cambridge Crystallographic Data Centre via www.ccdc.cam.ac.uk/data_request/cif.

Acknowledgements

This work was supported by the Deutsche Forschungsgemeinschaft (SFB 623). We thank Kerstin Brödner and Olena Tverskoy for experimental assistance, and Prof. Dr. Klaus Ditrich, BASF SE, for providing enantiopure arylethylamines.

[1] a) R. Takeuchi, M. Kashio, *Angew. Chem.* **1997**, *109*, 268; *Angew. Chem. Int. Ed.* **1997**, *36*, 263; b) J. P. Janssen, G. Helmchen, *Tetrahedron Lett.* **1997**, *38*, 8025.

[2] Reviews: a) H. Miyabe, Y. Takemoto, *Synlett* **2005**, 1641; b) R. Takeuchi, S. Kezuka, *Synthesis* **2006**, 3349; c) G. Helmchen, A. Dahnz, P. Dübon, M. Schelwies, R. Weihofen, *Chem. Commun.* **2007**, 675; d) G. Helmchen in *Iridium Complexes in Organic Synthesis* (Eds.: L. A. Oro, C. Claver), Wiley-VCH, Weinheim, **2009**, p. 211; e) J. F. Hartwig, L. M. Stanley, *Acc. Chem. Res.* **2010**, *43*, 1461; f) W.-B. Liu, J.-B. Xia, S.-L. You, *Top. Organomet. Chem.* **2012**, *38*, 155; g) P. Tosatti, A. Nelson, S. P. Marsden, *Org. Biomol. Chem.* **2012**, *10*, 3147.

[3] C. Welter, O. Koch, G. Lipowsky, G. Helmchen, *Chem. Commun.* **2004**, 896.

[4] C. A. Kiener, C. Shu, C. Incarvito, J. F. Hartwig, *J. Am. Chem. Soc.* **2003**, *125*, 14272.

[5] The exceptions are the reactions with *ortho*-substituted cinnamyl derivatives, which display low reactivity and low enantioselectivity. Fortunately, new ligands have been found that provide excellent results in the allylic alkylation reactions of these substrates; see: W.-B. Liu, C. Zheng, C.-X. Zhuo, L.-X. Dai, S.-L. You, *J. Am. Chem. Soc.* **2012**, *134*, 4812.

[6] a) S. Streiff, C. Welter, M. Schelwies, G. Lipowsky, N. Miller, G. Helmchen, *Chem. Commun.* **2005**, 2957; b) C. Welter, A. Dahnz, B. Brunner, S. Streiff, P. Dübon, G. Helmchen, *Org. Lett.* **2005**, *7*, 1239; c) Q.-F. Wu, H. He, S.-L. You, *J. Am. Chem. Soc.* **2010**, *132*, 11418.

[7] S. Spiess, C. Welter, G. Franck, J.-P. Taquet, G. Helmchen, *Angew. Chem.* **2008**, *120*, 7764; *Angew. Chem. Int. Ed.* **2008**, *47*, 7652.

[8] G. Franck, M. Brill, G. Helmchen, *Org. Synth.* **2012**, *89*, 55.

[9] a) G. Franck, K. Brödner, G. Helmchen, *Org. Lett.* **2010**, *12*, 3886; b) P. Tosatti, J. Horn, A. J. Canpbell, D. House, A. Nelson, S. P. Marsden, *Adv. Synth. Catal.* **2010**, *352*, 3153; c) M. Gärtner, S. Mader, K. Seehafer, G. Helmchen, *J. Am. Chem. Soc.* **2011**, *133*, 2072; d) K.-Y. Ye, H. He, W.-B. Liu, L.-X. Dai, G. Helmchen, S.-L. You, *J. Am. Chem. Soc.* **2011**, *133*, 19006; e) K.-Y. Ye, L.-X. Dai, S.-L. You, *Org. Biol. Chem.* **2012**, *10*, 5932.

[10] a) S. T. Madrahimov, D. Marković, J. F. Hartwig, *J. Am. Chem. Soc.* **2009**, *131*, 7228; b) D. Marković, J. F. Hartwig, *J. Am. Chem. Soc.* **2007**, *129*, 11680; c) S. T. Madrahimov, J. F. Hartwig, *J. Am. Chem. Soc.* **2012**, *134*, 8136.

[11] a) J. A. Raskatov, S. Spiess, C. Gnamm, K. Brödner, F. Rominger, G. Helmchen, *Chem. Eur. J.* **2010**, *16*, 6601; b) S. Spiess, J. A. Raskatov, C. Gnamm, K. Brödner, G. Helmchen, *Chem. Eur. J.* **2009**, *15*, 11087.

[12] R. Weihofen, O. Tverskoy, G. Helmchen, *Angew. Chem.* **2006**, *118*, 5673; *Angew. Chem. Int. Ed.* **2006**, *45*, 5546.

[13] T. Ohmura, J. F. Hartwig, *J. Am. Chem. Soc.* **2002**, *124*, 15164.

[14] T. Doi, A. Yanagisawa, M. Miyazawa, K. Yamamoto, *Tetrahedron: Asymmetry* **1995**, *6*, 389.

[15] Corresponding experiments with an analogous cod complex gave analogous results, see: S. Spiess, Dissertation, Universität Heidelberg, **2009**. Furthermore, the resting state of the alkylation with dimethyl malonate as a pronucleophile was also investigated with a dbcot complex as the catalyst. The (π-allyl)Ir complex was found as a resting state, as in the case of the cod complexes (see ref. [11a]).

[16] a) K. D. John, K. V. Salazar, B. L. Scott, R. T. Baker, A. P. Sattelberger, *Organometallics* **2001**, *20*, 296; b) B. Bartels, C. Garcia-Yebra, F. Rominger, G. Helmchen, *Eur. J. Inorg. Chem.* **2002**, 2569; c) C. García-Yebra, J. P. Janssen, F. Rominger, G. Helmchen, *Organometallics* **2004**, *23*, 5459.

[17] A. D. Becke, *J. Chem. Phys.* **1993**, *98*, 1372; A. D. Becke, *J. Chem. Phys.* **1993**, *98*, 5648.

[18] C. Lee, W. Yang, R. G. Parr, *Phys. Rev. B* **1988**, *37*, 785.

[19] Gaussian 03 (Revision B.03), M. J. Frisch, G. W. Trucks, H. B. Schlegel, G. E. Scuseria, M. A. Robb, J. R. Cheeseman, J. A. Montgomery, Jr., T. Vreven, N. Kudin, J. C. Burant, J. M. Millam, S. S. Iyengar, J. Tomasi, V. Barone, B Mennucci, M. Cossi, G. Scalmani, N. Rega, G. A. Petersson, H. Nakatsuji, M. Hada, M. Ehara, K. Toyota, R. Fukuda, J. Hasegawa, M. Ishida, T. Nakajima, Y. Honda, O. Kitao, H. Nakai, M. Klene, X. Li, J. E. Knox, H. P. Hratchian, J. B. Cross, V. Bakken, C. Adamo, J. Jaramillo, R. Gomperts, R. E. Stratmann, O. Yazyev, A. J. Austin, R. Cammi, C. Pomelli, J. W. Ochterski, P. Y. Ayala, K. Morokuma, G. A. Voth, P. Salvador, J. J. Dannenberg, V. G. Zakrzewski, S. Dapprich, A. D. Daniels, M. C. Strain, O. Farkas, D. K. Malick, A. D. Rabuck, K. Raghavachari, J. B. Foresman, J. V. Ortiz, Q. Cui, A. G. Baboul, S. Clifford, J. Cioslowski, B. B. Stefanov, G. Liu, A. Liashenko, P. Piskorz, I. Komaromi, R. L. Martin, D. J. Fox, T. Keith, M. A. Al-Laham, C. Y. Peng, A. Nanayakkara, M. Challacombe, P. M. W. Gill, B. Johnson, W. Chen, M. W. Wong, C. Gonzalez, J. A. Pople, Gaussian, Inc., Wallingford CT, **2004**.

[20] D. Andrae, U. Haeussermann, M. Dolg, H. Stoll, H. Preuss, *Theor. Chim. Acta* **1990**, *77*, 123.

[21] a) R. Ditchfield, W. J. Hehre, J. A. Pople, *J. Chem. Phys.* **1971**, *54*, 724; b) W. J. Hehre, R. Ditchfield, J. A. Pople, *J. Chem. Phys.* **1972**, *56*, 2257; c) P. C. Hariharan, J. A. Pople, *Theo Chim. Acta* **1973**, *28*, 213; d) P. C. Hariharan, J. A. Pople, *Mol. Phys.* **1974**, *27*, 209; e) M. S. Gordon, *Chem. Phys. Lett.* **1980**, *76*, 163.

[22] C. Y. Peng, H. B. Schlegel, *Isr. J. Chem.* **1994**, *33*, 449.

[23] C. Benzi, M. Cossi, V. Barone, R. Tarroni, C. Zannoni, *J. Phys. Chem. B* **2005**, *109*, 2584.

[24] J. Tomasi, B. Mennucci, R. Cammi, *Chem. Rev.* **2005**, *105*, 2999.

[25] H. E. Gottlieb, V. Kotylar, A. Nudelman, *J. Org. Chem.* **1997**, *62*, 7512.

[26] S. Berger, U. Zeller, *Angew. Chem.* **2004**, *116*, 2070.

 © 2012 Wiley-VCH Verlag GmbH & Co. KGaA, Weinheim

These are not the final page numbers!

[27] C. Gnamm, G. Franck, N. Miller, T. Stork, K. Brödner, G. Helmchen, *Synthesis* **2008**, 3331.
[28] C. Gnamm, S. Förster, N. Miller, K. Brödner, G. Helmchen, *Synlett* **2007**, 790.
[29] a) D. Polet, A. Alexakis, K. Tissot-Croset, C. Corminboeuf, K. Ditrich, *Chem. Eur. J.* **2006**, *12*, 3596; b) K. Tissot-Croset, D. Polet, A. Alexakis, *Angew. Chem.* **2004**, *116*, 2480; *Angew. Chem. Int. Ed.* **2004**, *43*, 2426.
[30] G. M. Sheldrick, SADABS 2008/1, Bruker Analytical X-ray Division, Madison, Wisconsin **2008**.
[31] SHELXTL 2008/4, G. M. Sheldrick, *Acta Crystallogr. Sect. A* **2008**, *64*, 112.

Received: May 19, 2012
Published online: ■■ ■■, 0000

 © 2012 Wiley-VCH Verlag GmbH & Co. KGaA, Weinheim

Reaction Mechanisms

*J. A. Raskatov, M. Jäkel, B. F. Straub, F. Rominger, G. Helmchen** ▮▮▮▮–▮▮▮▮

Iridium-Catalyzed Allylic Substitutions with Cyclometalated Phosphoramidite Complexes Bearing a Dibenzocyclooctatetraene Ligand: Preparation of (π-Allyl)Ir Complexes and Computational and NMR Spectroscopic Studies

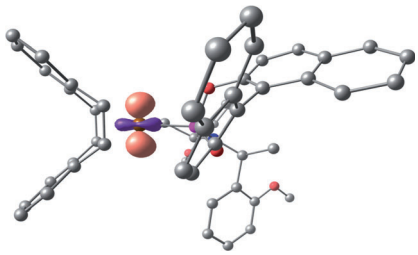

Bigger is better: The replacement of cod by dibenzo-cot is worth the effort because (allyl)Ir complexes of the latter compound are catalysts that give rise to improved regioselectivity and stability in iridium-catalyzed allylic aminations and alkylations.

© 2012 Wiley-VCH Verlag GmbH & Co. KGaA, Weinheim

These are not the final page numbers!